Neuron
Article

GABAergic Projection Neurons Route Selective Olfactory Inputs to Specific Higher-Order Neurons

Liang Liang,[1,2] Yulong Li,[3,5] Christopher J. Potter,[1,6] Ofer Yizhar,[4,7] Karl Deisseroth,[4] Richard W. Tsien,[3,8] and Liqun Luo[1,*]
[1]Department of Biology and Howard Hughes Medical Institute
[2]Department of Applied Physics
[3]Department of Molecular and Cellular Physiology
[4]Departments of Bioengineering and Psychiatry and Howard Hughes Medical Institute
Stanford University, Stanford, CA 94305, USA
[5]Current address: State Key Laboratory of Biomembrane and Membrane Biotechnology, College of Life Sciences and Peking-Tsinghua Center for Life Sciences, Peking University, Beijing 100871, China
[6]Current address: Solomon H. Snyder Department of Neuroscience, Johns Hopkins University School of Medicine, Baltimore, MD 21205, USA
[7]Current address: Department of Neurobiology, Weizmann Institute of Science, Rehovot 76100, Israel
[8]Current address: NYU Neuroscience Institute, New York University, New York, NY 10016, USA
*Correspondence: lluo@stanford.edu
http://dx.doi.org/10.1016/j.neuron.2013.06.014

SUMMARY

We characterize an inhibitory circuit motif in the *Drosophila* olfactory system, parallel inhibition, which differs from feedforward or feedback inhibition. Excitatory and GABAergic inhibitory projection neurons (ePNs and iPNs) each receive input from antennal lobe glomeruli and send parallel output to the lateral horn, a higher center implicated in regulating innate olfactory behavior. Ca^{2+} imaging of specific lateral horn neurons as an olfactory readout revealed that iPNs selectively suppressed food-related odor responses, but spared signal transmission from pheromone channels. Coapplying food odorant did not affect pheromone signal transmission, suggesting that the differential effects likely result from connection specificity of iPNs, rather than a generalized inhibitory tone. Ca^{2+} responses in the ePN axon terminals show no detectable suppression by iPNs, arguing against presynaptic inhibition as a primary mechanism. The parallel inhibition motif may provide specificity in inhibition to funnel specific olfactory information, such as food and pheromone, into distinct downstream circuits.

INTRODUCTION

Inhibition occurs throughout the nervous system, impacting diverse processes like spinal cord reflexes (Sherrington, 1906), receptive field formation of the retinal ganglion cells (Kuffler, 1953), and cortical representations of sensory information (Isaacson and Scanziani, 2011). In many well-studied circuits, inhibition is local, carried out by GABAergic neurons that lie close to the brain areas on which they exert their functions. Long-range communication between different brain regions is instead often conveyed by excitatory neurons. There are also notable examples of long-distance-projecting GABAergic neurons, such as cerebellar Purkinje cells and striatal spiny projection neurons. In both cases, GABAergic neurons constitute the sole output from the brain regions where their cell bodies reside. In this study, we analyze a paradigm in the fly olfactory system in which excitatory and GABAergic projection neurons each receive input from antennal lobe glomeruli and send parallel output to overlapping regions in a higher-order olfactory center, the lateral horn.

The *Drosophila* olfactory system (Figure 1A) is a well-established and genetically tractable model system for studying how sensory information is processed to produce internal representations of the outside world (reviewed in Liang and Luo, 2010; Olsen and Wilson, 2008a; Su et al., 2009; Vosshall and Stocker, 2007). Odors are first recognized by a large repertoire of olfactory receptors, each of which is expressed in a specific class of olfactory receptor neurons (ORNs). ORNs expressing a given odorant receptor project their axons to one of ~50 stereotypic glomeruli in the antennal lobe, where their axons synapse with dendrites of the corresponding class of projection neurons (PNs). This organization creates ~50 parallel information-processing channels. An extensive network of local interneurons (LNs) in the antennal lobe receive input from ORNs and PNs and send output back to ORN axon terminals, PN dendrites, or other LNs. The actions of these LNs contribute to the transformation of odor representations between ORNs and PNs (e.g., Bhandawat et al., 2007; Olsen et al., 2010). The mammalian olfactory system shares many of these properties and organizational principles, highlighting a common solution to odor representation in the brain (Bargmann, 2006).

An outstanding question is how olfactory inputs direct innate and learned behavior. The axons from the excitatory PNs (ePNs) relay olfactory information to the mushroom body, a center for olfactory learning and memory (Davis, 2005; Heisenberg,

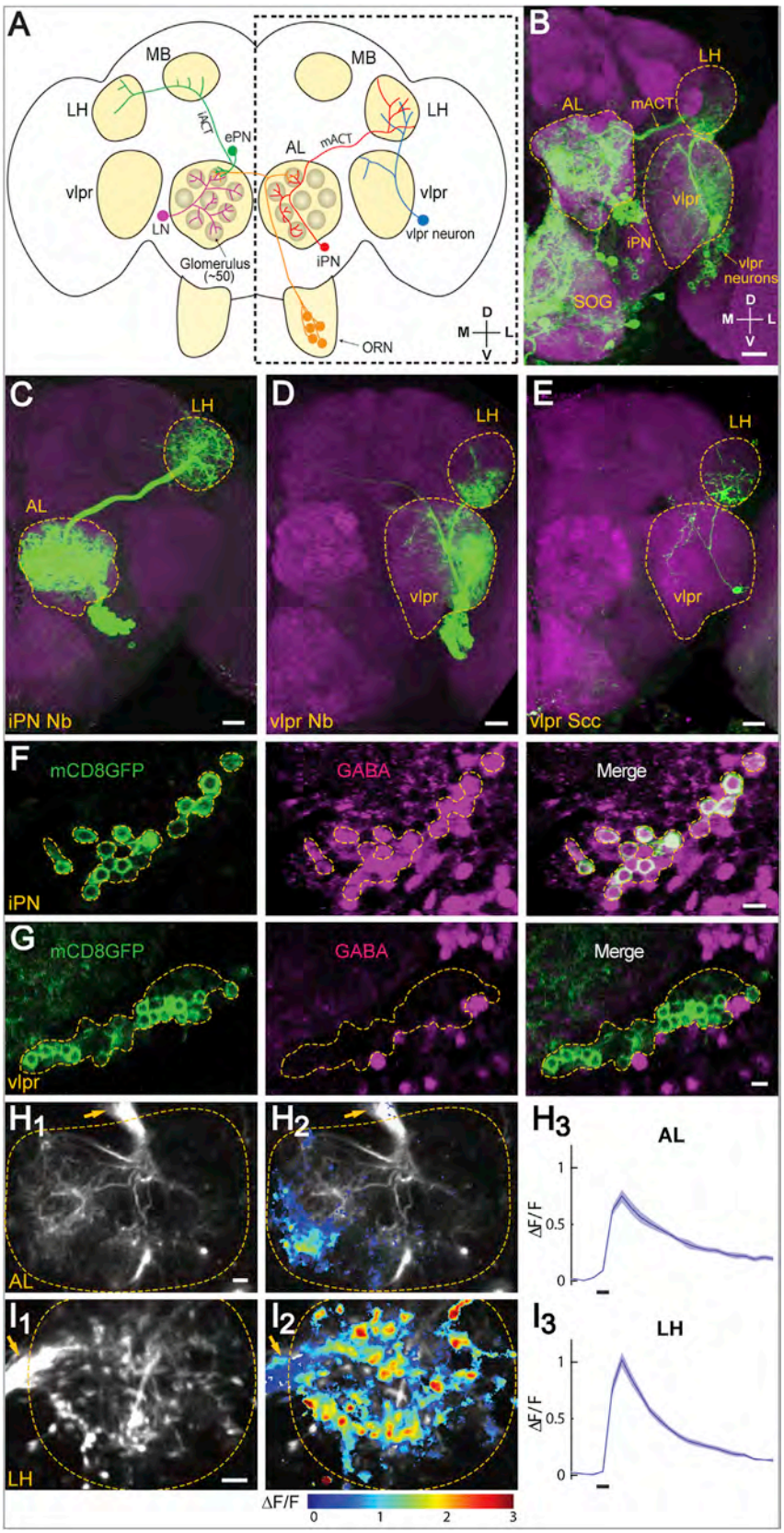

Figure 1. Characterization of *Mz699-GAL4+* Inhibitory Projection Neurons and vlpr Neurons

(A) Schematic diagram of the fly olfactory system. Odor is first detected by olfactory receptor neurons (ORNs, orange), which send axons to the antennal lobe (AL) in both hemispheres and synapse with dendrites of projection neurons (PNs) and local interneurons (LNs, purple). Excitatory PNs (ePNs, green) project their axons through the inner antennocerebral tract (iACT) to the mushroom body (MB) and lateral horn (LH). Inhibitory PNs (iPNs, red) send axons through the middle antennocerebral tract (mACT) to innervate the LH only. Also shown is a class of putative third-order neurons (blue) that connects the LH with the ventrolateral protocerebrum (vlpr). The area outlined by the dotted box is shown in (B)–(E). D, dorsal; V, ventral; M, medial; L, lateral.

(B) *Mz699-GAL4* is expressed in iPNs, vlpr neurons, and neurons that innervate the subesophageal ganglion (SOG) as revealed by the *UAS-mCD8GFP* reporter. We occasionally observed Mz699+ neurons (0–2 per hemisphere) lateral to the lateral horn neuropil, which send processes into the dorsal lateral horn. Because of inconsistent and weak expression, we did not further consider these neurons in this study. Green: anti-GFP staining; magenta: monoclonal antibody (mAb) nc82 staining of the general neuropil. Scale = 20 μm.

(C–E) MARCM analysis allowed separate visualization of an iPN neuroblast clone (C), a vlpr neuroblast clone (D), or a vlpr single-cell clone (E). Green: anti-GFP staining; magenta: anti-N-Cadherin staining of the general neuropil. Scale = 20 μm.

(F and G) The inhibitory neurotransmitter GABA is present in the majority of iPNs (F) but absent in the vlpr neurons (G). Green: anti-mCD8 staining (driven from *Mz699-GAL4*); magenta: anti-GABA. Scale = 5 μm.

(H and I) Ca^{2+} imaging of *Mz699-GAL4*-driven GCaMP3 expression in the antennal lobe (H) and lateral horn (I) (outlined) in response to 0.1% isoamyl acetate. Arrows point to the mACT. Scale = 5 μm. Averaged basal fluorescence at the AL (H_1) and LH (I_1). Normalized fluorescence changes ΔF/F (1 = 100%) are superimposed on the averaged basal fluorescence (H_2 and I_2). Time courses of ΔF/F over the region with positive Ca^{2+} signals (H_3 and I_3). Odor durations (500 ms) are indicated as horizontal bars below. Mean ± SEM (three repeats). See Figure S1 for more on MARCM analysis of Mz699+ neurons and Figure S2 for more on iPN response in the antennal lobe.

2003), and to the lateral horn, a less-understood higher-order center presumed to direct olfaction-mediated innate behavior (Heimbeck et al., 2001). Indeed, the terminal arborization patterns of PN axons within the lateral horn are highly stereotyped according to PN glomerular class, whereas their innervation patterns in the mushroom body are much more variable (Jefferis et al., 2007; Marin et al., 2002; Tanaka et al., 2004; Wong et al., 2002). Interestingly, presynaptic terminals for PNs that represent food odors and pheromones are spatially segregated in the lateral horn (Jefferis et al., 2007), but little is known about how olfactory inputs are transformed from PNs to higher-order lateral horn neurons (Ruta et al., 2010).

Thus far, most physiological and behavioral studies of *Drosophila* PNs have focused on the uniglomerular ePNs, which reside dorsal and lateral to the antennal lobe and whose axons form the inner antenno-cerebral tract (iACT), innervating both the mushroom body and the lateral horn (Figure 1A). However, a separate group of PNs reside ventral to the antennal lobe. Individual ventral PNs send dendrites to either single or multiple glomeruli and project their axons through the middle antenno-cerebral tract (mACT) to terminate only in the lateral horn, bypassing the mushroom body altogether (Jefferis et al., 2007; Lai et al., 2008; Okada et al., 2009; Stocker et al., 1990). In this study, we use the olfactory response of a specific set of higher-order neurons to show that these ventral PNs provide GABAergic inhibition in the lateral horn to route selective inputs to specific higher-order neurons.

RESULTS

Mz699-GAL4 Allows Genetic Access to Ventral PNs and vlpr Lateral Horn Neurons

Ventral PNs of the antennal lobe have previously been characterized using two GAL4 lines. *GH146-GAL4* labels ~6 ventral PNs (Jefferis et al., 2001), all of which are GABAergic (Jefferis et al., 2007), and all are uniglomerular except one that innervates all glomeruli (Marin et al., 2002). *Mz699-GAL4* labels >45 ventral PNs that are mostly complementary to those labeled by *GH146-GAL4* (Lai et al., 2008). Most *Mz699-GAL4*-positive (Mz699+ hereafter) ventral PNs project to multiple glomeruli (Lai et al., 2008) and more than 80% are GABAergic (Okada et al., 2009). *Mz699-GAL4* also labels neurons in the ventrolateral protocerebrum (vlpr) that send processes into the lateral horn (Okada et al., 2009; Figure 1B).

To further characterize neurons labeled by *Mz699-GAL4*, we used mosaic analysis with a repressible cell marker (MARCM)-based clonal analysis (Lee and Luo, 1999). Consistent with a previous study (Lai et al., 2008), we found that Mz699+ ventral PNs were derived from a single neuroblast (Figure 1C; Figure S1A). Most single-cell clones innervated a few glomeruli (Figure S1B; n = 38 out of 39), which collectively covered the majority of glomeruli. We also introduced synaptotagmin-hemagglutinin (Syt-HA) as a synaptic vesicle marker in these MARCM clones and found that Syt-HA was highly enriched in the lateral horn but was largely absent from the antennal lobe in neuroblast and single-cell clones (Figures S1A–S1C). This is consistent with a previous report based on the labeling of all Mz699+ neurons (Okada et al., 2009). With single-cell resolution, we observed that the majority of the ventral PN (vPN) neural processes in the antennal lobe had fine terminal branches without Syt-HA signal (Figure S1B), whereas Syt-HA puncta, likely representing presynaptic terminals of en passant synapses, were distributed throughout the branches in the lateral horn (Figure S1C). These data suggest that Mz699+ ventral PNs deliver olfactory information from the antennal lobe to the lateral horn. Consistent with a previous report (Okada et al., 2009), we found that the vast majority of Mz699+ ventral PNs were GABAergic based on GABA staining (Figure 1F; 87.6% ± 2.5% GABA positive, from 8 antennal lobes with an average of 55 cells per lobe). As described later, the ventral PNs provide inhibition that requires GABA synthesis. Thus, we refer to them hereafter as inhibitory PNs (iPNs) to distinguish them from the excitatory PNs (ePNs) from the anterodorsal and lateral lineages.

Additionally, we examined Mz699+ vlpr neurons that also project to the lateral horn as putative higher-order neurons in the olfactory pathway. Neuroblast and single-cell clone analyses of vlpr neurons showed that a subset projected to the lateral horn as well as the vlpr neuropil (Figures 1D and 1E). Both processes were enriched for Syt-HA (Figures S1D and S1E), similar to several other lateral horn neurons, including those that connect the lateral horn to the vlpr (Jefferis et al., 2007). Furthermore, in the single-cell clone of vlpr neurons, Syt-HA+ puncta are distributed through the processes in the vlpr neuropil including most of the terminals. In the lateral horn, however, the neural processes end with fine branches without Syt-HA puncta (Figure S1E). This result suggests that Mz699+ vlpr neurons mostly send information from the lateral horn to the vlpr neuropil. Thus, these lateral horn-projecting Mz699+ vlpr neurons represent a subset of putative third-order neurons in the lateral horn. None of the Mz699+ vlpr neurons were GABA positive (Figure 1G). Below, we used their odor-evoked response as a means to investigate the role of iPN function in olfactory signal processing.

iPNs Are Activated by Odors

To investigate the function of iPNs, we first examined their odor responses utilizing two-photon Ca^{2+} imaging in alert flies labeled by *Mz699-GAL4* driving *UAS-GCaMP3* (Tian et al., 2009). When we applied 500 ms pulses of 0.1% isoamyl acetate (IA), a major component of the banana odor, to the antennae, we observed a robust increase of Ca^{2+} signals in the antennal lobe (Figure 1H; Figure S2A), the lateral horn (Figure 1I), and the mACT tract before it enters the lateral horn neuropil (Figure 1I, arrow). Application of 1% apple cider vinegar gave similar results (data not shown; see below). We further tested Ca^{2+} response of iPNs to IA applied at different concentrations in the antennal lobe (Figures S2C and S2E). At low IA concentration, the response was sparse and weak. As the odor concentration increased, more glomeruli were recruited with elevated Ca^{2+} signals, similar to the concentration-dependent odor responses of ORN and ePN (Hallem and Carlson, 2006; Wang et al., 2003).

Because the neuronal elements that express GCaMP3 in the antennal lobe were derived exclusively from dendrites of Mz699+ iPNs, we conclude that iPNs are activated by odors, likely through ORN→iPN synapses in the antennal lobe glomeruli, although it is possible that iPNs are instead or additionally activated by ePNs. At the same time, through their

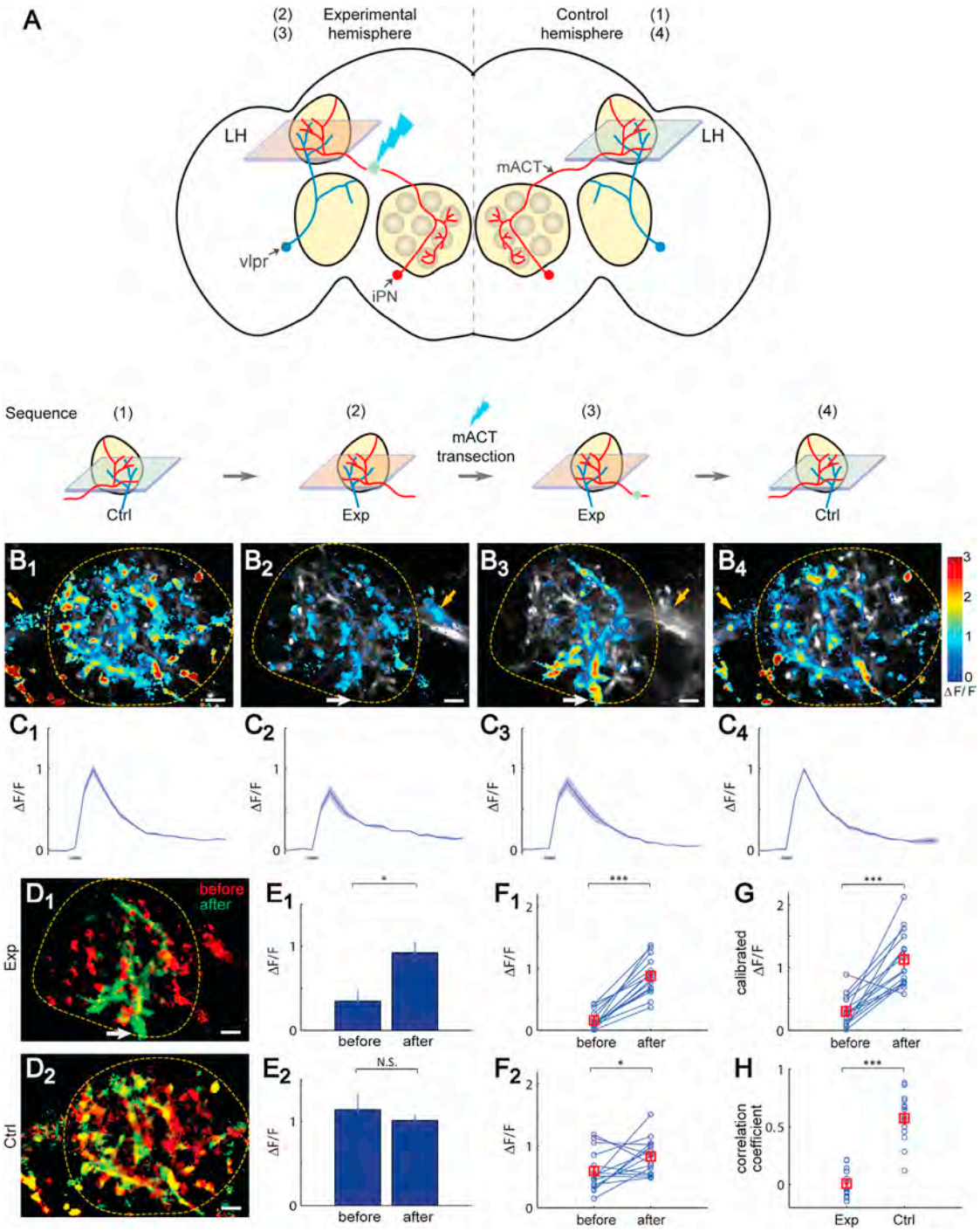

Figure 2. Lateral Horn Response of vlpr Neurons to Isoamyl Acetate Is Inhibited by iPNs via the mACT Projection

(A) Schematic diagram of the experimental procedures to dissect iPN and vlpr Ca^{2+} responses in the lateral horn (LH). Ctrl, control hemisphere; Exp, experimental hemisphere. The sequence of the experimental procedures is outlined at the bottom, which corresponds to the images and time course in (B) and (C).

(B) Isoamyl acetate (IA)-induced Ca^{2+} signals corresponding to each step above from a representative fly. The lateral horn is outlined. Yellow arrows point to the mACT prior to its entry into the lateral horn. White arrows point to the entry site of vlpr dendrites into the lateral horn. After transection, Ca^{2+} signals disappeared from the mACT but appeared at the vlpr dendrites (compare B_3 with B_2). The differences between (B_1) and (B_2) are due to images taken at different focal planes of the lateral horn in the control and experimental hemispheres.

(C) Time course of the corresponding ΔF/F in (B_1)–(B_4). Odor durations (500 ms) are indicated as horizontal bars below. Mean ± SEMs (three repeats).

(D) Overlay of the before- (red) and after-transection (green) Ca^{2+} signals for experimental (D_1) and control (D_2) hemispheres. The spatial patterns of green and red are distinct in (D_1) but overlap extensively in (D_2).

(legend continued on next page)

mACT axonal projection, iPNs effectively send olfactory signals to the lateral horn (see below).

Acute mACT Transection Distinguishes the iPNs and vlpr Responses at the Lateral Horn

Since both iPNs and vlpr neurons send processes to the lateral horn, IA-elicited Ca^{2+} signals within the lateral horn (Figure 1I) could be contributed by either or both of these neuronal types. We next aimed to isolate putative postsynaptic signals of vlpr neurons from presynaptic signals in iPNs within the same lateral horn using a laser transection protocol outlined in Figure 2A. Specifically, we first obtained lateral horn odor responses from control and experimental hemispheres. We then used Mz699-labeled iPN axons as a guide and applied spatially confined laser pulses from the two-photon laser (Ruta et al., 2010) to transect the mACT prior to its entry to the lateral horn on the experimental hemisphere. Following the laser transection, we again imaged lateral horn odor responses in both experimental and control hemispheres.

Several lines of evidence suggested that our laser transection of mACT was complete and specific. First, we could observe a small cavitation bubble at the mACT from basal GCaMP3 fluorescence with our two-photon microscope immediately following the laser application (Figure S3A), a hallmark of laser transection (Vogel and Venugopalan, 2003). Second, retrospective immunostaining validated the complete transection of the mACT (Figure S3B, n = 15) with no visible effect on the integrity of the nearby iACT that conveys signals from the ePNs (data not shown). Third, odor-evoked GCaMP3 signals in mACT near the lateral horn entry site (e.g., Figure $2B_2$, yellow arrow) were invariably abolished after laser transection of mACT (Figure $2B_3$, yellow arrow), validating that the responses observed in intact preparations were due to iPN contributions and were lost after mACT transection. Fourth, applying the same energy from the two-photon laser at locations away from mACT did not cause similar changes in lateral horn Ca^{2+} signals (data not shown). Fifth, we did not detect changes of iPN responses in the antennal lobe before or after mACT transection (data not shown), suggesting that olfactory input still activates iPNs in the antennal lobe after mACT transection. Thus, we could assume that olfactory response in the lateral horn neuropil after mACT transection is mostly contributed by the vlpr neurons.

mACT Transection Revealed that iPNs Normally Inhibit vlpr Responses to Isoamyl Acetate

How does iPN projection contribute to olfactory information processing at the lateral horn, and specifically, how are the responses of putative third-order vlpr neurons modulated by iPN input? To address these questions, we compared Ca^{2+} signals in response to isoamyl acetate application in the lateral horn (referred to as IA response hereafter) before and after laser transection (Figures 2B and 2C). In all cases, IA responses in the lateral horn were robust (Figure 2C). However, a striking change occurred in the spatial patterns in the experimental hemisphere (compare Figures $2B_3$ and $2B_2$). Before transection, the IA response was scattered across the lateral horn (Figure $2B_2$). After transection, IA response appeared most intense in the ventral lateral horn near the lateral horn entry site of vlpr dendrites (Figure $2B_3$, white arrow). This change of spatial pattern was evident when we superimposed the IA response before and after transection on the same lateral horn (Figure $2D_1$). By contrast, the spatial patterns of IA response in the control hemisphere appeared similar before and after mACT transection (compare Figures $2B_1$ and $2B_4$; Figure $2D_2$).

We used two approaches to quantitatively analyze the changes of IA response before and after mACT transection. In the first approach, we defined a region of interest (ROI) based on the spatial pattern of the after-transection IA response for each imaging plane (see Supplemental Experimental Procedures). In the control hemisphere, this ROI encompasses the activated regions of both iPNs and vlpr neurons. In the experimental hemisphere, however, this ROI would correspond to activated regions of vlpr neurons only, since iPN input was eliminated after mACT transection. We then quantified $\Delta F/F$ signals within the ROI for the IA responses before and after transection. In the experimental hemisphere, the after-transection response was significantly increased compared to that before transection (Figure $2E_1$), suggesting that most after-transection responses in the ROI (i.e., vlpr neuronal responses) were newly gained as a consequence of mACT transection. This difference was highly significant across individual flies (Figure $2F_1$).

To rule out the contribution of olfactory adaptation or potential nonspecific deterioration of fly physiology during the imaging procedure, we used the lateral horn IA response in the control hemisphere from the same fly as an internal control. The magnitude of the IA response in the lateral horn remained unchanged in the example fly (Figure $2E_2$). Although across flies there was a slight increase in the control hemisphere after transection compared with before (Figure $2F_2$; see Supplemental Experimental Procedures for a likely cause), when we used calibrated responses (IA responses within ROI of the experimental hemisphere divided by that of the control hemisphere from the

(E) Peak $\Delta F/F$ values before or after transection within the region of interest (ROI) as defined by the spatial pattern after transection (green in D). The vlpr response exhibited a significant increase on the experimental side (three repeats; $p < 0.05$; t test), but not on the control side (three repeats).

(F) Paired comparisons of $\Delta F/F$ before and after mACT transection across different flies (n = 15). The experimental hemisphere shows a highly significant increase of vlpr responses after transection (paired t test) (F_1). The control hemisphere shows a slight, but significant, increase (F_2). With two-way repeated-measures ANOVA, mACT transection, brain hemisphere (experimental versus control), and their interaction are all statistically significant ($p < 0.001$; $p < 0.01$; $p < 0.001$, respectively).

(G) Calibrated $\Delta F/F$ of vlpr responses (experimental hemisphere divided by the control hemisphere for the same fly) exhibited a significant increase after transection (paired t test).

(H) Each circle represents the correlation coefficient of spatial patterns before and after mACT transection for an individual fly. There is little correlation on the experimental hemisphere (mean = 0.067), but high correlation on the control hemisphere (mean = 0.516). The correlation coefficient between the two groups is significantly different (paired t test). For all statistical analyses in this and subsequent figures, error bars represent ±SEM. *$p < 0.05$; **$p < 0.01$; ***$p < 0.001$; N.S. (not significant), $p > 0.05$. See Figure S2 for validation of mACT transection and Figure S6 for dependence of vlpr response to IA concentration.

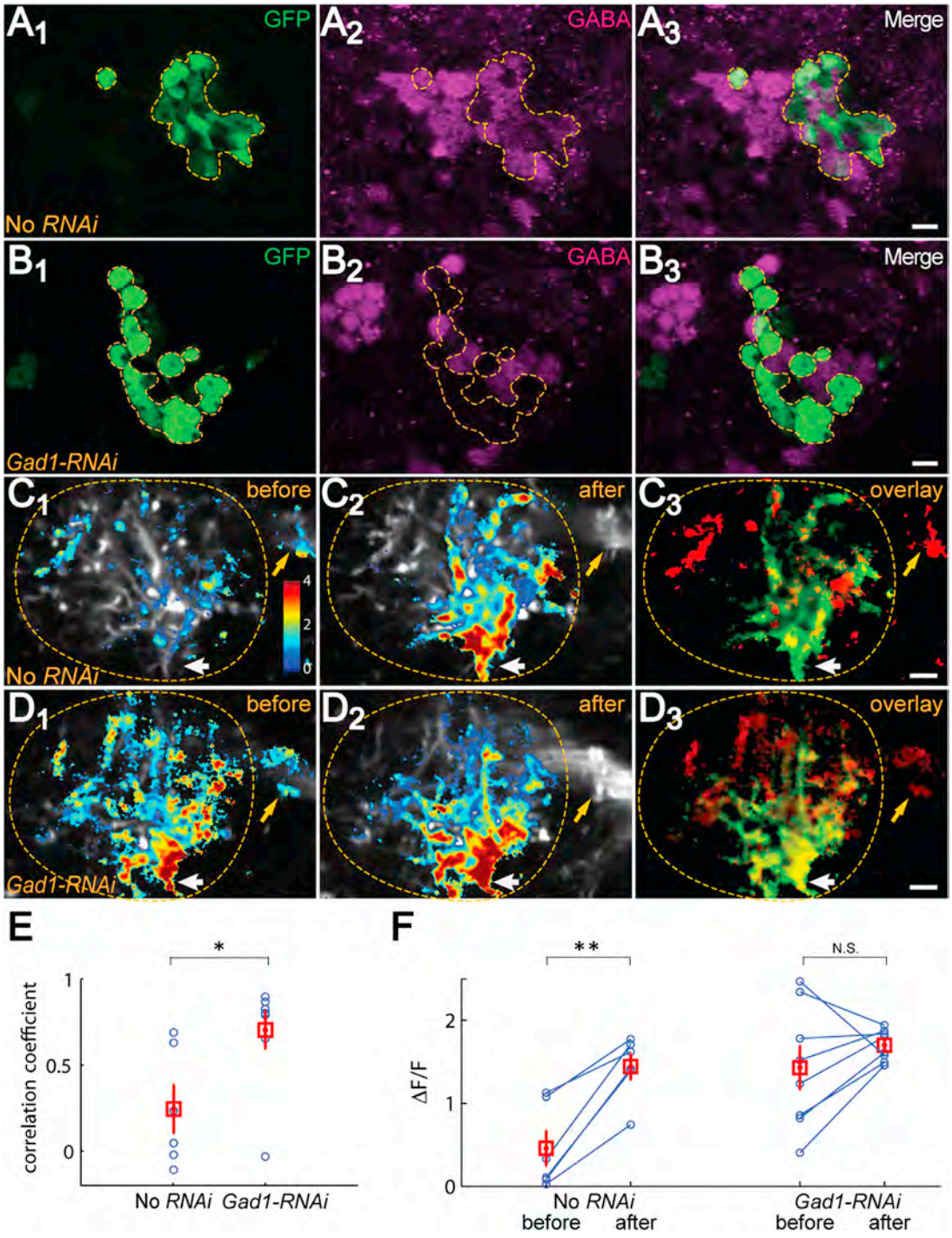

Figure 3. Blocking GABA Synthesis in iPNs Suppresses iPN Inhibition of vlpr Neurons

(A and B) Compared with No-*RNAi* control (A), *Gad1-RNAi* expression caused a loss of GABA staining in Mz699+ neurons (B). Magenta, anti-GABA; green, anti-GFP. The confocal images are from single z planes. Scale = 5 μm.

(C and D) Compared with No *RNAi* (C_1), fly expressing *Gad1-RNAi* in Mz699+ neurons shows greatly enhanced IA response in the lateral horn (D_1) before mACT transection. mACT transection induced robust changes in the intensity and spatial pattern of IA responses in control (compare C_2 with C_1), including the loss of mACT signal (yellow arrows) and the gain of signals at the vlpr dendrite entry site (white arrows). By contrast, mACT transection did not cause robust increases in IA response (D_2) nor change the spatial pattern in the *Gad1-RNAi* fly (compare D_2 with D_1), except the signal loss at the mACT (yellow arrows). ΔF/F of Ca^{2+} signals are superimposed on the averaged raw images. (C_3) and (D_3) are an overlay of Ca^{2+} signals before (red) and after (green) mACT transection for (C_1) and (C_2) and (D_1) and (D_2), respectively. Lateral horns are outlined. Scale = 5 μm.

(legend continued on next page)

same fly), IA response increase was highly significant across individual flies after mACT transection (Figure 2G).

In the second approach, we analyzed the correlation of spatial patterns of IA response before and after mACT transection (see Supplemental Experimental Procedures). The control hemisphere showed a high correlation (Figure 2H, right column), consistent with the resemblance of their spatial activity patterns before and after transection. By contrast, the experimental hemisphere exhibited a significantly smaller correlation coefficient (Figure 2H, left column) compared to the control hemisphere. This smaller correlation coefficient likely reflected combined effects of a loss of iPN response and gain of vlpr response.

Taken together, these data indicate that while the iPN contribution to the lateral horn IA response was abolished as a result of mACT transection, there was an additional, highly significant gain of IA response in the vlpr neurons after mACT transection. This suggests that the vlpr response to IA stimulation is normally inhibited by iPN projections through the mACT.

Blocking GABA Synthesis in iPNs Suppresses iPN Inhibition of vlpr Neurons

To test whether GABA release mediates the observed inhibitory signals from the mACT onto the vlpr lateral horn neurons, we perturbed GABA synthesis from iPNs by introducing *UAS-Gad1-RNAi* in conjunction with *UAS-Dicer2* into our imaging flies (*Mz699-GAL4, UAS-GCaMP3*) to knock down glutamic acid decarboxylase 1 (Gad1), the critical enzyme responsible for GABA biosynthesis (Küppers et al., 2003). Immunostaining revealed no detectable GABA in 49 out of 51 Mz699+ neurons under the experimental condition (Figure 3B; compared to control in Figure 3A). Although the *Gad1 RNAi* transgene was also expressed in Mz699+ vlpr neurons, these neurons should be unaffected since they were not GABAergic (Figure 1G).

Control flies (no *UAS-Gad1-RNAi*) exhibited general elevation and a spatial pattern change of IA response in the lateral horn after mACT transection (Figure 3C_2) compared with before (Figure 3C_1), as we have described (Figure 2). However, Gad1 knockdown in iPNs resulted in a robust lateral horn IA response in intact flies, with a spatial pattern that resembled IA response after mACT transection (Figure 3D_1). Specifically, in intact Gad1 knockdown flies, IA robustly activated the ventral lateral horn near the vlpr dendrite entry site (Figure 3D_1, white arrow), a region that normally exhibited robust IA response only after transection in control flies. mACT transection no longer resulted in significant spatial pattern changes, as shown by the representative images (Figures 3D_2 and 3D_3) and by a higher correlation coefficient of spatial patterns before and after mACT transection compared with controls (Figure 3E). Using ROIs defined by after-transection patterns to isolate vlpr responses, we found a statistically significant interaction between the fly genotype and mACT transection. Separate statistical tests on the ablation effect showed no statistically significant change in Gad1 knockdown flies before and after mACT transection, in contrast to the increase of IA response in control animals after mACT transection (Figure 3F).

Together, these experiments indicate that GABAergic inhibition from the mACT is largely responsible for the suppression of IA responses of vlpr neurons under physiological conditions. The phenotypic similarity between mACT transection and Gad1 knockdown in Mz699+ neurons also suggests that Mz699+ neurons provide the major inhibitory input through the mACT to the lateral horn in our experimental context.

iPN Inhibition of vlpr Neurons Is Odor Dependent

Our results thus far suggest that GABA release from iPNs inhibits IA responses of higher-order vlpr neurons. Do iPNs inhibit all odors similarly? To address this question, we used the same paradigm and analysis method (Figure 2) to examine the Ca^{2+} response of vlpr neurons to several other odors.

We first examined apple cider vinegar, a natural attractant for flies that has been used for physiological and behavioral experiments (Semmelhack and Wang, 2009). We found similar results as IA, both qualitatively and quantitatively (Figure 4A, compared with Figure 2). Specifically, there was a marked increase of vinegar responses in new regions of the lateral horn after mACT transection (Figures 4A_1–4A_3). The correlation coefficient for spatial patterns before and after mACT transection was significantly smaller in the experimental hemisphere compared to the control hemisphere (Figure 4A_4). Using ROIs created from after-transection patterns to isolate the vlpr response, we found a significant increase of vlpr vinegar response after mACT transection in the experimental, but not control, hemisphere (Figure 4A_5).

Next, we examined the lateral horn responses triggered by optogenetic stimulation of Or67d ORNs, which are activated by a well-characterized pheromone, 11-*cis*-vaccenyl acetate (cVA) (Ejima et al., 2007; Kurtovic et al., 2007; van der Goes van Naters and Carlson, 2007). Activating these neurons largely recapitulates behavioral responses to cVA (Kurtovic et al., 2007). To optimize light responses in expressing neurons, we used a channelrhodopsin variant that contained both the H134R mutation that increases photocurrent sizes (Nagel et al., 2005) and the C128T mutation that slows the channel photocycle (Berndt et al., 2009). The resulting $ChR2_{TR}$ channels showed robust photocurrents in cultured mammalian neurons and triggered spiking with high light sensitivity in vivo (Figure S4). To genetically access two neuronal populations independently for optogenetic stimulation and Ca^{2+} imaging, we utilized the Q system (Potter et al., 2010) to express $ChR2_{TR}$ in Or67d neurons (Figures S5A and S5B). Blue light stimulation induced a robust and specific Ca^{2+} response of ePNs in the DA1 glomerulus, the target of Or67d ORN axons (Figure S5C), supporting the potency and specificity of optogenetic activation. We also characterized iPN antennal

(E) The spatial patterns of the ΔF/F in the lateral horn before and after laser transection are highly correlated in individual *Gad1-RNAi* flies and, as a group, are significantly different from the No-*RNAi* group (t test).

(F) Paired comparison of ΔF/F before and after transection across flies. After-transection patterns were used to define an ROI for quantification to isolate the vlpr response. With two-way repeated-measures ANOVA, mACT transection, genotype, and their interaction are all statistically significant ($p < 0.01$; $p < 0.05$; $p < 0.05$, respectively). No-*RNAi* flies exhibited a significant increase after mACT transection compared with before, but no significant change was observed for *Gad1-RNAi* flies. *Gad1-RNAi*: n = 8; No-*RNAi*: n = 6.

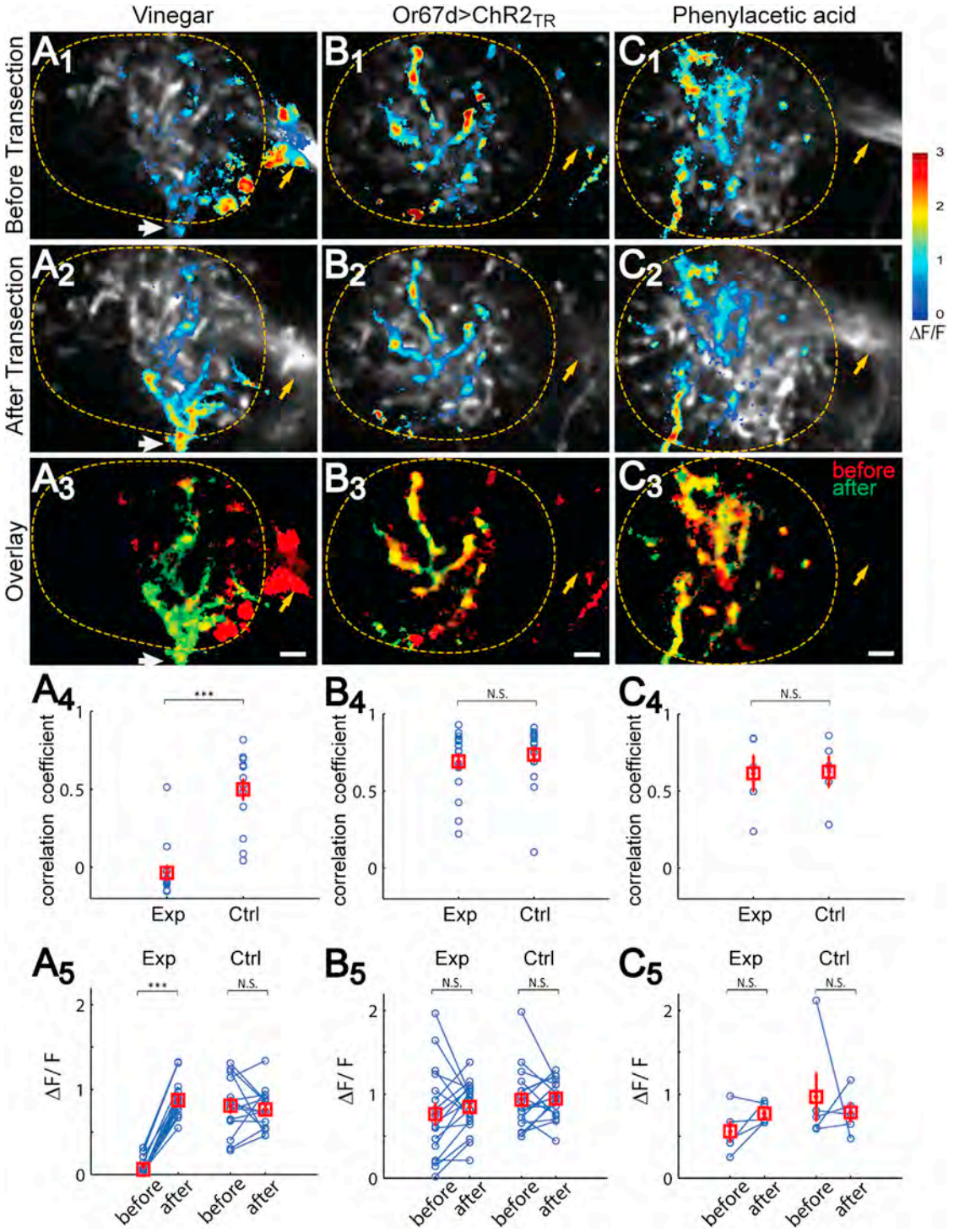

Figure 4. iPN Inhibition of vlpr Neurons Is Odor Specific

(A–C) Ca^{2+} responses to 1% apple cider vinegar (A), optogenetic activation of Or67d ORNs (B), and 1% phenylacetic acid (PAA) (C) are shown as representative images before (A_1, B_1, and C_1) or after (A_2, B_2, and C_2) mACT transection. Their overlay is shown in (A_3), (B_3), and (C_3). Whereas the spatial patterns of vinegar response change drastically after mACT transection, including signal loss in mACT (yellow arrows) and signal gain in vlpr dendrite entry site at the ventral lateral (white arrows), few changes are seen in Or67d and PAA responses before and after transection. Lateral horns are outlined. Scale = 5 μm. Correlation coefficients of spatial patterns of Ca^{2+} response for before- and after-transection (A_4, B_4, and C_4). For vinegar, the average correlation before versus after is close to 0 and significantly smaller than that in the control hemisphere (paired t test) (A_4). For Or67d and PAA stimuli, the correlation coefficients in experimental hemispheres are comparable to the control hemispheres. Quantification of ΔF/F across different animals for the three stimuli in ROI created by after-transection responses (A_5, B_5,

(legend continued on next page)

lobe responses to different levels of optogenetic activation of Or67d ORNs. iPN signals are restricted to the DA1 glomerulus and increased with increasing laser power from 0.012 to 0.12 mW/mm^2 (Figures S2B, S2D, and S2F).

We chose the 0.06 mW/mm^2 as the laser power to activate Or67d ORNs and examined the lateral horn Ca^{2+} response (referred to as Or67d responses hereafter). We found a robust Or67d response (Figure 4B$_1$), which is dependent on the presence of the ChR2$_{TR}$ transgene. In contrast to the marked gain of new regions for IA or vinegar responses after mACT transection (Figures 2 and 4A), the spatial patterns of Or67d responses appeared similar before and after mACT transection (Figure 4B). This can be seen by the minimal changes from superimposition of the spatial patterns (Figure 4B$_3$ compared with Figures 4A$_3$ and 2D$_1$), similar correlation coefficient in the experimental and control hemispheres (Figure 4B$_4$), and similar Ca^{2+} response magnitudes before and after transection using an ROI defined by the after-transection response (Figure 4B$_5$). Together, these data suggest that Or67d activation led to robust vlpr neuronal response in intact flies and that this response was not significantly inhibited by iPNs.

To test whether other olfactory-processing channels behave similarly to Or67d, we tested phenylacetic acid (PAA), which is derived from food but enhances male courtship (Grosjean et al., 2011). PAA activates mostly Ir84a-expressing ORNs that project to the VL2a glomerulus (Grosjean et al., 2011; Silbering et al., 2011). The axonal projections of VL2a PNs in the lateral horn exhibit more similarities to pheromone-representing, rather than food-representing, PNs, consistent with its function in promoting mating behavior (Grosjean et al., 2011). We found that the lateral horn responses of *Mz699-GAL4, UAS-GCaMP3* flies to PAA resembled those of Or67d activation: the responses exhibited strong similarity before and after mACT transection (Figure 4C), suggesting that PAA normally activates vlpr neurons, and this activation is minimally inhibited by iPNs. Thus, using olfactory response of vplr neurons as the readout, our data suggest a difference in iPN inhibition of food- versus pheromone-related odor-processing channels, though we cannot rule out the possibility that the difference is due to simultaneously activating multiple glomeruli in the case of IA or vinegar and stimulating single glomeruli in the case of Or67d or PAA.

To examine whether the odor-selective iPN inhibition is affected by stimulus intensity, we performed additional experiments with varying stimulus strengths. We found that lateral horn responses to higher or lower concentrations of IA than our original concentration (10^{-3}) were both elevated after mACT transection, although a higher concentration of IA (3×10^{-3}) evoked Ca^{2+} response of vlpr neurons in some intact animals (Figure S6A). By contrast, mACT transection did not affect the dose-response curve of Or67d stimulation (Figure S6B). These experiments suggest that the differential inhibition is dependent on the nature of the odorants, rather than a consequence of different levels of excitation by these different odors.

The Or67d→vlpr Processing Channel Is Insulated from iPN Inhibition

Of the above four stimuli we have examined, IA and vinegar responses of vlpr neurons were robustly inhibited by iPNs, whereas the responses to Or67d or PAA stimulation were not. We envisioned two contrasting models that could account for these differences. In the first model, which we termed "bulk inhibition" (Figure 5A), iPN inhibition is nonselective and proportional to the number of iPNs that are excited by the odor. Since IA or vinegar each activate many glomeruli (Semmelhack and Wang, 2009; Wang et al., 2003), they should also activate a large number of iPNs, and therefore send a strong bulk inhibitory signal to the lateral horn (Figure 5A$_1$). By contrast, Or67d neurons or PAA stimulation each activates a single glomerulus, and therefore engages a smaller number of iPNs, with limited inhibitory tone in the lateral horn (Figure 5A$_2$). In the alternative model, which we termed "selective inhibition" (Figure 5B), the Or67d- or PAA-processing channel is insulated from iPN inhibition that applies to the IA and vinegar-processing channels.

These two models have different predictions if we were to costimulate Or67d neurons with IA. If the bulk inhibition model was correct, the lateral horn Or67d response (mostly contributed by vlpr neurons) would be diminished with IA coapplication in intact animals, as IA application would activate many iPNs and send a strong inhibitory signal to the lateral horn (Figure 5A$_3$). Alternatively, if the selective inhibition model was true, the Or67d response would not change with IA coapplication (Figure 5B$_3$).

We thus compared the lateral horn responses to IA, Or67d, and IA + Or67d in the same fly. Activating Or67d neurons by optogenetic means simplified the experimental paradigm and circumvented possible peripheral odor-odor interactions (Su et al., 2011) or cross-contamination of residual odors during odor delivery. We measured lateral horn odor response to IA, Or67d neuronal activation, and costimulation in intact animals for 3–6 iterations (Figure 5C). To test whether Or67d neuronal responses would be inhibited by IA coapplication, we isolated the ROI of vlpr response to Or67d stimulation by performing mACT transection (Figure 5D). Within the ROI, we found that costimulation of IA did not cause a detectable change of Or67d response magnitude in intact flies (Figures 5E–5G), despite the fact that IA clearly activated lateral horn responses outside the ROI (Figures 5C$_1$ and 5C$_3$). This experiment provided strong support to the selective inhibition model, at least for the cVA-processing channel.

and C$_5$). mACT transection leads to a drastic increase in vlpr neuron response to vinegar stimulation (n = 14, paired t test), but not to OR67d > ChR2$_{TR}$ (n = 17) or PAA (n = 5) stimulation. In all cases, Ca^{2+} signals in the control hemisphere are not significantly changed. With two-way repeated-measures ANOVA, mACT transection, brain hemisphere (experiment versus control), and their interaction are all statistically significant ($p < 0.001$) to vinegar stimulation, but none are statistically significant for Or67d > ChR2$_{TR}$ or PAA stimulation. See Figure S2 for Or67d > ChR2$_{TR}$ characterization in the antennal lobe, Figure S4 for characterization in mammalian neurons, Figure S5 for characterization of *Or67d-QF* and *QUAS-ChR2$_{TR}$* transgenes, and Figure S6 for dependence of vlpr response to Or67d > ChR2$_{TR}$ stimulation intensity.

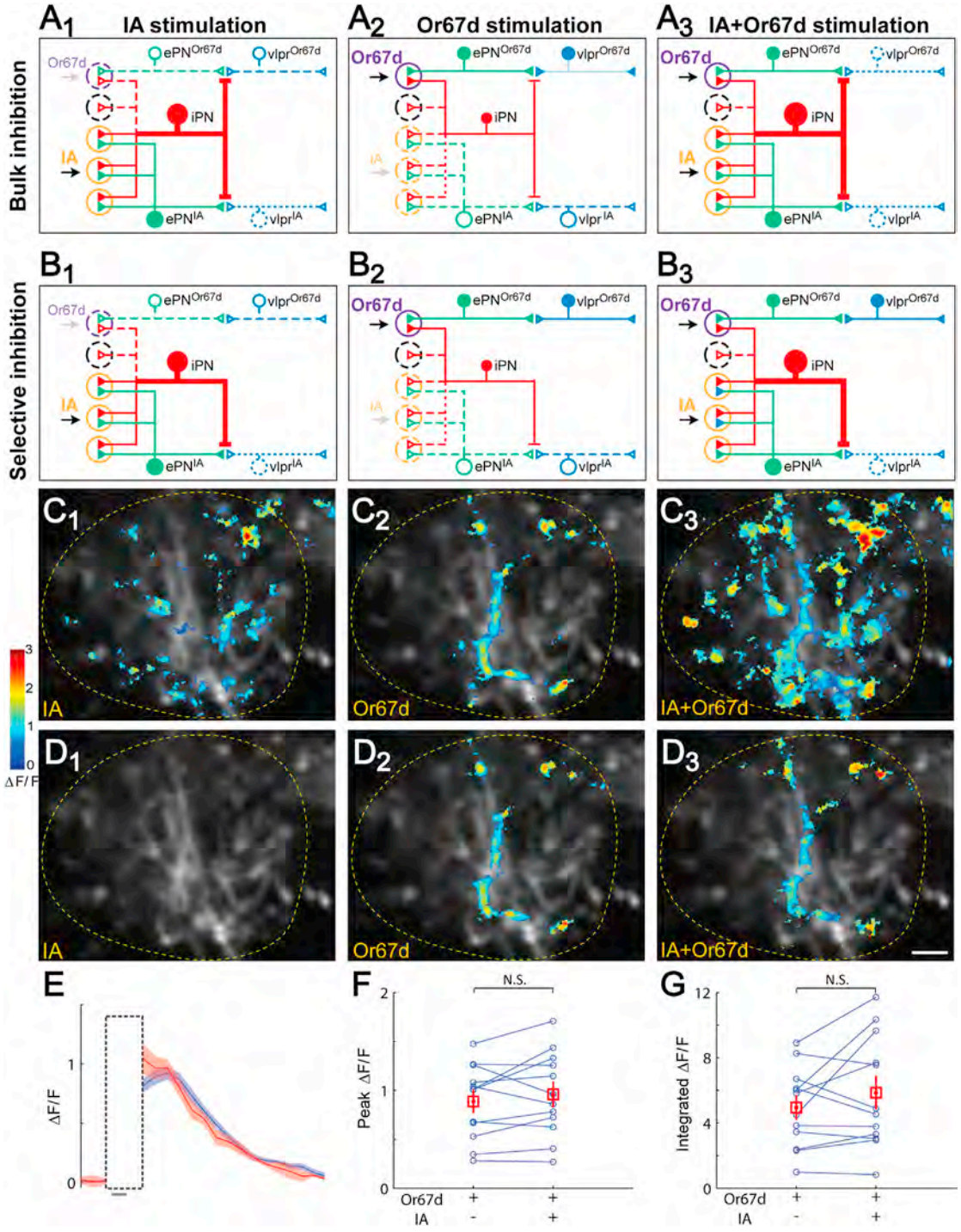

Figure 5. vlpr Response to Or67d Activation Is Not Inhibited by Coapplication of IA

(A) In the bulk inhibition model, iPNs as a whole (represented by a single red neuron) inhibit all vlpr responses nondiscriminately, but the strength of inhibition (represented by the size of the iPN) is proportional to the number of activated glomeruli. IA stimulation (A_1) causes stronger inhibition than Or67d stimulation (A_2) because IA activates more glomeruli (orange circle) than Or67d (purple circle). IA + Or67d costimulation is predicted to decrease vlpr response to Or67d (A_3). In the schematic shown here and in (B), solid neurons represent active neurons; dotted neurons are not activated and/or are inhibited.

(B) In the selective inhibition model, iPN inhibition is processing-channel selective. Specifically, iPNs inhibit vlpr responses to IA (B_1), but not to Or67d (B_2), stimulation. Hence, IA + Or67d costimulation is predicted to not affect vlpr response to Or67d (B_3).

(C) Ca^{2+} responses of the same fly to IA (C_1), OR67d > $ChR2_{TR}$ (C_2), and IA + OR67d > $ChR2_{TR}$ (C_3). Each image is the average of three raw images from three iterations of first IA, followed by alternating Or67d and IA + Or67d stimulations.

(legend continued on next page)

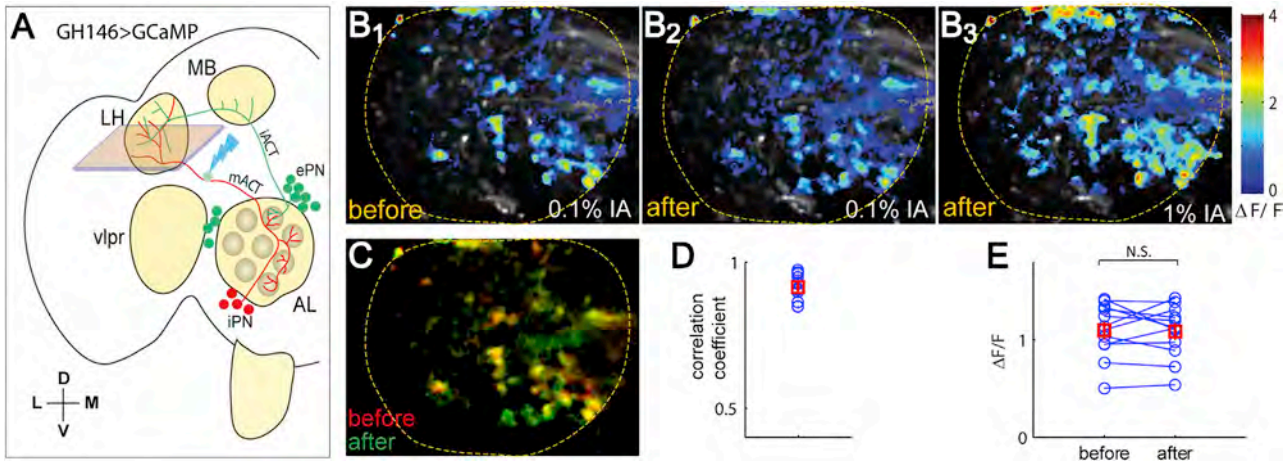

Figure 6. Presynaptic Ca^{2+} Signals of ePNs Are Not Affected by mACT Transection

(A) In *GH146-GAL4, UAS-GCaMP3* flies, lateral horn Ca^{2+} signal in intact flies is a sum of ~90 ePNs and 6 iPNs. After mACT transection (guided by iPN axons), lateral horn Ca^{2+} signal is contributed by ePNs only, which should be elevated compared to intact flies if iPNs act by presynaptic inhibition, but remain mostly unchanged if iPNs do not inhibit ePNs presynaptically (five of the six iPNs are uniglomerular iPNs that innervate glomeruli not activated by IA; see Jefferis et al., 2007).

(B) In a representative fly, 0.1% IA evoked robust response in the axon terminals of PNs in intact fly (B_1). There was no apparent change of response pattern after the mACT transection (B_2). Delivery of 1% IA at the end of the experiment elevated ePN response (B_3), indicating that 0.1% IA did not saturate the PN response.

(C) Overlay of the Ca^{2+} signals before and after mACT transection in the example fly.

(D) The spatial patterns of before and after laser transection showed high correlation.

(E) The peak ePN response to 0.1% IA was not changed after mACT transection across flies (n = 12) in an ROI defined by the spatial pattern after laser transection.

Evidence against Presynaptic Inhibition of ePNs as the Primary Mechanism of iPN Action

The lateral horn neuropil is composed of axon terminals from ePNs and iPNs as well as dendrites of putative third-order neurons, including the vlpr neurons. In principle, iPN inhibition of vlpr response could be caused by a direct inhibition of vlpr neurons, presynaptic inhibition of ePNs, or a combination of both. Ca^{2+} imaging does not have sufficient temporal resolution to discern whether the vlpr neurons receive direct iPN input. However, we could examine the contribution of presynaptic inhibition of ePNs by comparing Ca^{2+} imaging of ePN terminals before and after mACT transection. If there was presynaptic inhibition on ePN terminals, and the inhibition occurred at the step of or before presynaptic Ca^{2+} entry that triggers neurotransmitter release as most GABA-mediated inhibition does, we would expect an elevated Ca^{2+} response to the same olfactory stimulation after mACT transection.

To test if ePN presynaptic Ca^{2+} signals are normally inhibited by iPNs, we used *GH146-GAL4* to drive GCaMP3 expression, since this GAL4 labels the majority of ePNs that allowed us to image Ca^{2+} response of IA at their axon terminals as well as a few iPNs that allowed us to target mACT for transection (Figure 6A). We found that the Ca^{2+} responses in the lateral horn were similar before and after mACT transection (compare Figures 6B_1 and 6B_2) in both their spatial patterns (Figures 6C and 6D) and response magnitude (Figure 6E). The lack of elevation of Ca^{2+} signal in response to mACT transection was not due to saturation of GCaMP3 sensors in the ePN axon terminal, as this response was elevated by stimulation with a higher IA concentration (Figure 6B_3). These data argue against the presynaptic inhibition mediated by reduction of Ca^{2+} influx as a primary mechanism for iPN inhibition.

DISCUSSION

Two general circuit motifs involving inhibitory neurons are widely used in vertebrate and invertebrate nervous systems. In feedback inhibition (Figure 7A), inhibitory neurons are locally activated by excitatory neurons. In turn, they inhibit a broad array of excitatory neurons, including those that excite them. In feedforward inhibition (Figure 7B), excitatory input activates both excitatory and inhibitory target neurons, and the activated inhibitory target neurons further inhibit the excitatory target neurons. The mammalian olfactory bulb, for instance, provides examples of both motifs. As an example of feedback inhibition, granule cells are activated by mitral cells in response to odor stimuli. In turn, they inhibit the same and neighboring mitral cells. As an example of feedforward inhibition, ORN axons

(D) Ca^{2+} responses as in (C), shown only for regions within an ROI that isolates vlpr response to Or67d stimulation. This ROI was determined by after-transection Or67d response subtracting its small overlap with the IA response before transection to ensure that only the vlpr response to Or67d stimulation was quantified. Lateral horns are outlined. Scale = 5 μm.

(E) Averaged ΔF/F over time for the response to OR67d > $ChR2_{TR}$ (blue) and to coapplication with IA (red) (mean ± SEM, three repeats). Gray bar at the bottom indicates the 500 ms optogenetic and/or odor stimulation duration. The vertical box represents the time at which imaging was turned off to avoid sensing the light from the $ChR2_{TR}$-activating blue laser.

(F and G) Quantification of the peak (F) and integrated (G) ΔF/F response. In both cases, Or67d response was not affected by IA costimulation (n = 12).

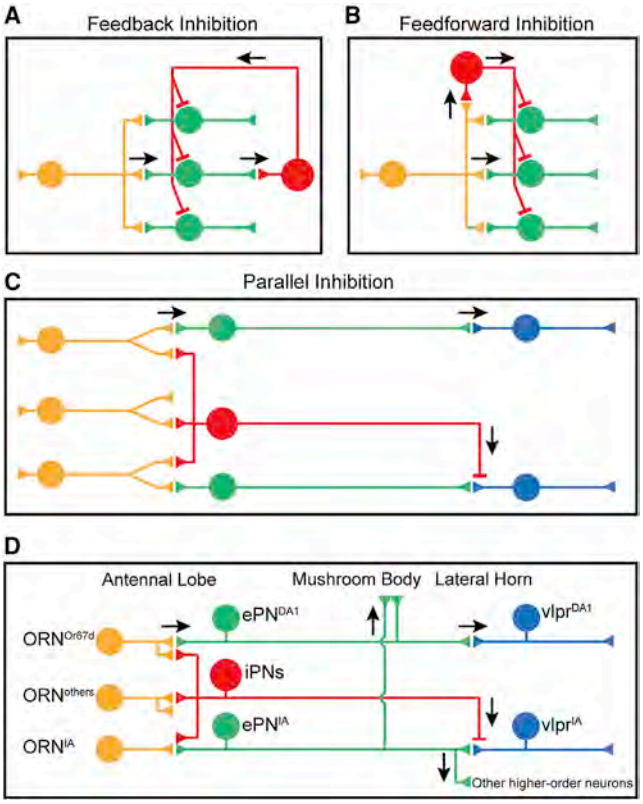

Figure 7. Inhibitory Circuit Motifs and Schematic Summary

(A–C) Schematic for feedback inhibition (A), feedforward inhibition (B), and parallel inhibition (C). Arrows indicate the direction of signal flow. See Discussion for details.

(D) Schematic summary of the current study. From the perspective of the Mz699+ vlpr olfactory response, iPNs function via a parallel inhibition strategy to suppress vlpr activities elicited by food odors, but not pheromones. ePN^{IA} presumably also activate other higher-order neurons to elicit foraging behavior (bottom right). Likewise, ePN^{DA1} also activate other higher-order neurons (not shown; see Ruta et al., 2010). In contrast to ePNs, which send collaterals to the mushroom body, iPNs project axons only to the lateral horn.

excite periglomerular cells and mitral cells in parallel; some periglomerular cells inhibit mitral cells in the same and adjacent glomeruli. Both granule cells and periglomerular cells contribute to the lateral inhibition and sharpening of the olfactory signals that mitral cells deliver to the olfactory cortex (Shepherd et al., 2004). Similarly, the fly antennal lobe, the equivalent of the mammalian olfactory bulb, has a diversity of GABAergic local interneurons (LNs) (Chou et al., 2010). Some LNs are excited by ORNs and subsequently provide feedback inhibition onto ORN axon terminals for gain control (Olsen and Wilson, 2008b; Root et al., 2008). Other LNs may act on PN dendrites for feedforward inhibition. Here we describe an inhibitory circuit motif that differs from classic feedforward and feedback inhibition, which we term parallel inhibition (Figure 7C), wherein excitatory and inhibitory projection neurons receive parallel input and send parallel output to a common target region (the lateral horn; Figure 7D).

What are the possible roles of iPNs, and what advantages might the parallel inhibition motif confer? By monitoring olfactory responses of a subset of putative third-order lateral horn neurons (the vlpr neurons) and by laser transecting the ascending mACT input from iPNs while sparing ePNs, we showed that iPNs selectively route olfactory input to vlpr neurons. Specifically, the vlpr responses to the food odors are inhibited by the iPNs, but the response to the cVA pheromone-processing channel is not subjected to this inhibition (Figure 7D). Previous anatomical studies revealed highly stereotyped branching and terminal arborization patterns for uniglomerular ePNs and iPNs (Jefferis et al., 2007; Lai et al., 2008). Results in this study provide functional demonstration that GABAergic iPNs regulate olfactory inputs to the lateral horn neurons. Indeed, the fact that removing iPN inhibition allows IA and vinegar signals to activate vlpr neurons suggests that anatomical segregation of PN axon terminals representing food and pheromone (Jefferis et al., 2007) alone is not sufficient to prevent food odors to activate vlpr neurons, at least some of which are normally activated by pheromones. iPN inhibition provides another level of specificity of the higher-order neuronal responses to olfactory input.

This specificity of inhibition provides a special feature of parallel inhibition (Figures 7C and 7D) in comparison with feedforward and feedback inhibition (Figures 7A and 7B). Feedforward and feedback inhibition tend to be nonspecific with respect to their target population within the same neuronal type, which is optimal for certain functions these motifs serve, such as lateral inhibition and gain control (Isaacson and Scanziani, 2011). In the *Drosophila* antennal lobe, for example, while exhibiting a large variety of arborization patterns, most LNs innervate many to all glomeruli, where they both receive input and send output (Chou et al., 2010). By contrast, the specific dendritic glomerular innervation of individual iPNs in the antennal lobe, as well as their stereotyped axonal arborization patterns in the lateral horn, enable iPNs to selectively inhibit some olfactory-processing channels, but not others (Figure 7D). We speculate that food odors should activate other lateral horn higher-order neurons relevant to foraging and that such activation is not strongly inhibited by iPNs, perhaps also due to inhibition specificity (Figure 7D, bottom right).

Another interesting feature of parallel inhibition is the timing of inhibition. Inhibition from feedforward and certainly feedback motifs arrive later than excitation due to transmission through an extra synapse, which is used to confine the magnitude and/or duration of excitation (Buzsáki, 1984; Isaacson and Scanziani, 2011). The parallel inhibition motif in principle allows for simultaneous arrival of excitation and inhibition at the postsynaptic neurons, potentially enabling inhibition to completely suppress excitation, and is ideally suited for information gating. We provided evidence that the primary action of iPNs is unlikely through presynaptic inhibition of ePNs, as ePN presynaptic Ca^{2+} signals in response to olfactory stimuli were not elevated by mACT transection. A caveat of this interpretation is that some forms of presynaptic inhibition can bypass Ca^{2+} entry, for instance through $G\beta\gamma$ action on the release machinery (Gerachshenko et al., 2005); however, we are not aware of GABAergic inhibition that acts in this manner. Thus, we favor the idea that iPNs act directly on postsynaptic third-order neurons under our experimental conditions. Due to the limited temporal resolution of Ca^{2+} imaging, we have not explored the temporal property of parallel

inhibition in this study. It will be interesting for future research to measure the arrival time of both excitatory and inhibitory input directly with more sensitive and temporally precise electrophysiological methods.

Here, we describe the use of the parallel inhibition motif in sensory systems. Long-distance GABAergic projections are prevalent in the mammalian brain (see Introduction). Specifically, some GABAergic neurons in the hippocampus and cortex have recently been identified that send long-distance projections, sometimes to the same area as the glutamatergic projection neurons (Higo et al., 2009; Jinno et al., 2007; Melzer et al., 2012). Thus, parallel inhibition can potentially be a widely used mechanism in the nervous system.

We identified a unique class of higher-order neurons that respond to Or67d (and presumably cVA) activation. Or67d ORNs and their postsynaptic partner DA1 excitatory PNs express Fru^M, a male-specific transcription factor that is a key regulator of sexual behavior (Manoli et al., 2005; Stockinger et al., 2005). A previous study identified a number of Fru+ higher-order cVA-responsive neurons whose cell bodies reside dorsal and lateral to the lateral horn (Ruta et al., 2010). Indeed, the analyses of Fru+ neurons have so far provided many examples where Fru+ neurons are connected with each other to regulate different aspects of sexual behavior (Dickson, 2008; Yu et al., 2010). However, lateral horn-projecting Mz699+ vlpr neurons do not appear to express Fru^M (data not shown), despite their robust activation by Fru+ Or67d ORNs. This may reflect a broad function of cVA as a pheromone that regulates not only mating but also aggression (Wang and Anderson, 2010) and social aggregation (Bartelt et al., 1985).

Our study revealed a difference between food- and pheromone-processing channels in their susceptibility to inhibition by iPNs and suggests that pheromone channels may be insulated from general inhibition by iPNs. It is almost certain that iPNs play additional functions than reported here, as we only examined iPN function from the perspective of their effect on the olfactory response of a specific subset of higher-order neurons. Indeed, in a companion manuscript, Parnas et al. (2013) showed that iPNs play an instrumental role in facilitating the discrimination of mostly food odors, as assayed by quantitative behavioral experiments. Taken together, these studies uncovered two distinct aspects of iPN function: increased discrimination of diverse food odors and information gating between qualitatively different olfactory stimuli.

Finally, it is notable that of the two major ePN targets, iPN axons only project to the lateral horn but spare the mushroom body (Figure 7D). The mushroom body is a well-documented center for olfactory learning and memory, whereas PN projections to the lateral horn are implicated in regulating innate olfactory behavior (Heimbeck et al., 2001) (see also Parnas et al., 2013). ePN axons exhibit striking stereotypy in their terminal arborization patterns in the lateral horn, but not in the mushroom body (Caron et al., 2013; Jefferis et al., 2007; Marin et al., 2002; Wong et al., 2002). Recent anatomical tracing in mice also revealed differential input organization in distinct olfactory cortical areas (Miyamichi et al., 2011; Sosulski et al., 2011), suggesting a common principle in olfactory systems of insects and mammals. The selective innervation by iPNs of targeting neurons in the lateral horn suggests that regulation of innate olfactory behavior engages an additional level of specific inhibition to ensure that olfactory information carrying different biological values, such as food and pheromone, is funneled into distinct downstream circuits, resulting in the activation of distinct behavioral outputs.

EXPERIMENTAL PROCEDURES

Ca^{2+} Imaging of Odor Response

Two-photon GCaMP imaging experiments were performed with either a LSM 510 Two-Photon Laser-Scanning Confocal Microscope (Zeiss) with a 40× NA 0.8 water-immersion objective (Zeiss) and modelocked Ti:Sapphire laser (Coherent) tuned to 920 nm or a customized two-photon microscope (Prairie Technologies) with a 40× NA 1.0 water-immersion objective (Zeiss) and laser tuned to 927 nm at ~73–75°F. The excitation power at the specimen was ~10 mW, and the pixel dwell time was 2.0 μs. All lateral horn images were acquired at a 2.488 Hz frame rate with 460 × 300 pixels per frame. Each imaging cycle was 45 s, and 500 msec odor stimuli (as determined by the solenoid valves) were always delivered at 5 s. To minimize bleaching, images were only taken from the first 16 s (40 frames) of each cycle. In most experiments, the same odor was applied every other cycle for three repeats, while different odors were usually applied in an alternate manner to minimize potential olfactory adaptation. Image acquisition was suspended during the 500 msec optogenetic stimulation period to protect the PMTs. On average, each imaging session lasted ~1.5 hr, with most of the flies appearing healthy at the end of the experiments; they could still move their legs at a regular pace. For some experiments, the fly brains were dissected and fixed for post hoc staining.

Time-lapse imaging series of GCaMP3 from a single z plane were usually recorded in the control hemisphere once before mACT transection and once after transection. On the experimental hemisphere, three different z planes were recorded both before and after transection in most experiments to maximize the likelihood of capturing vlpr processes in the imaging plane. The z plane with the largest area of vlpr responses after laser transection was used for image analysis.

Optogenetic Stimulation

Flies of the genotype *Or67d-QF/y; UAS-GCaMP3, QUAS-ChR2$_{TR}$; Mz699-Gal4/+* were used for optogenetic stimulation of Or67d ORNs. Adult male flies were collected 0–2 days after eclosion and transferred to new vials containing 10 g instant fly food (Carolina Biological, Formula 4-24) dissolved in 500 ml 5 mM all trans-Retinal (Sigma, R2500) and kept in a dark, humidified container at room temperature. Flies were transferred to a new vial of such food every 2 days for ~8–10 days before imaging. $ChR2_{TR}$ was activated by a 473 nm diode-pumped blue solid-state laser (CrystaLaser 60 mW). The blue laser was coupled to an optical fiber for light delivery. The other end of the fiber was screwed into a connector mounted on the fly chamber so as to deliver the same light power for each experiment. The same TriggerSync plugin (Prairie Technologies) was used to synchronize the laser activation and image acquisition. For each imaging cycle, optogenetic stimulation was on between 5 s and 5.5 s.

Laser Transection

Guided by the GCaMP3 basal-level fluorescence at 927 nm, we first defined a transection window (~4 μm × 3 μm, at zoom ×10 and in a single focal plane) centered on the mACT about 10 μm before its entry site into the lateral horn. A ~80 mW laser pulse (measured after the objective) at 800 nm was then applied onto this window. The pulse contains 16 repetitions of continuous frame scanning with a pixel dwell time of 8 μs and a total estimated energy of 0.04 J. Successful transection usually resulted in a small cavitation bubble formed in the mACT as reported before (Vogel and Venugopalan, 2003).

Supplemental Experimental Procedures contain additional sections on genetics and molecular biology, MARCM analysis and immunostaining, preparing flies for Ca^{2+} imaging, and data analysis.

SUPPLEMENTAL INFORMATION

Supplemental Information includes Supplemental Experimental Procedures and six figures and can be found with this article online at http://dx.doi.org/10.1016/j.neuron.2013.06.014.

ACKNOWLEDGMENTS

We thank Y. Chou, B. Dickson, V. Jayaraman, T. Lee, L. Looger, K. Wehner, X. Yu, the Bloomington Stock Center, the Vienna *Drosophila* RNAi Center, the Developmental Studies Hybridoma Bank, and the BACPAC Resources Center for fly stocks, reagents, and antibodies; S. Sinha, D. Profitt, and D. Luginbuhl for technical assistance; K. Beier, X. Chen, T. Clandinin, X. Gao, N. Makki, A. Mizrahi, T. Mosca, and R. Wilson for providing critiques of the manuscript; M. Schnitzer for support; and G. Miesenböck for communicating data prior to publication. This work is supported by an NIH grant (R01-DC005982 to L. Luo). L. Liang has been supported by a Stanford Graduate Fellowship and a Lubert Stryer Stanford Interdisciplinary Graduate Fellowship. L. Luo is an investigator of the Howard Hughes Medical Institute.

Accepted: June 4, 2013
Published: September 4, 2013

REFERENCES

Bargmann, C.I. (2006). Comparative chemosensation from receptors to ecology. Nature *444*, 295–301.

Bartelt, R.J., Schaner, A.M., and Jackson, L.L. (1985). cis-Vaccenyl acetate as an aggregation pheromone in Drosophila melanogaster. J. Chem. Ecol. *11*, 1747–1756.

Berndt, A., Yizhar, O., Gunaydin, L.A., Hegemann, P., and Deisseroth, K. (2009). Bi-stable neural state switches. Nat. Neurosci. *12*, 229–234.

Bhandawat, V., Olsen, S.R., Gouwens, N.W., Schlief, M.L., and Wilson, R.I. (2007). Sensory processing in the Drosophila antennal lobe increases reliability and separability of ensemble odor representations. Nat. Neurosci. *10*, 1474–1482.

Buzsáki, G. (1984). Feed-forward inhibition in the hippocampal formation. Prog. Neurobiol. *22*, 131–153.

Caron, S.J., Ruta, V., Abbott, L.F., and Axel, R. (2013). Random convergence of olfactory inputs in the Drosophila mushroom body. Nature *497*, 113–117.

Chou, Y.H., Spletter, M.L., Yaksi, E., Leong, J.C., Wilson, R.I., and Luo, L. (2010). Diversity and wiring variability of olfactory local interneurons in the Drosophila antennal lobe. Nat. Neurosci. *13*, 439–449.

Davis, R.L. (2005). Olfactory memory formation in Drosophila: from molecular to systems neuroscience. Annu. Rev. Neurosci. *28*, 275–302.

Dickson, B.J. (2008). Wired for sex: the neurobiology of Drosophila mating decisions. Science *322*, 904–909.

Ejima, A., Smith, B.P., Lucas, C., van der Goes van Naters, W., Miller, C.J., Carlson, J.R., Levine, J.D., and Griffith, L.C. (2007). Generalization of courtship learning in Drosophila is mediated by cis-vaccenyl acetate. Curr. Biol. *17*, 599–605.

Gerachshenko, T., Blackmer, T., Yoon, E.J., Bartleson, C., Hamm, H.E., and Alford, S. (2005). Gbetagamma acts at the C terminus of SNAP-25 to mediate presynaptic inhibition. Nat. Neurosci. *8*, 597–605.

Grosjean, Y., Rytz, R., Farine, J.P., Abuin, L., Cortot, J., Jefferis, G.S., and Benton, R. (2011). An olfactory receptor for food-derived odours promotes male courtship in Drosophila. Nature *478*, 236–240.

Hallem, E.A., and Carlson, J.R. (2006). Coding of odors by a receptor repertoire. Cell *125*, 143–160.

Heimbeck, G., Bugnon, V., Gendre, N., Keller, A., and Stocker, R.F. (2001). A central neural circuit for experience-independent olfactory and courtship behavior in Drosophila melanogaster. Proc. Natl. Acad. Sci. USA *98*, 15336–15341.

Heisenberg, M. (2003). Mushroom body memoir: from maps to models. Nat. Rev. Neurosci. *4*, 266–275.

Higo, S., Akashi, K., Sakimura, K., and Tamamaki, N. (2009). Subtypes of GABAergic neurons project axons in the neocortex. Front Neuroanat *3*, 25.

Isaacson, J.S., and Scanziani, M. (2011). How inhibition shapes cortical activity. Neuron *72*, 231–243.

Jefferis, G.S.X.E., Marin, E.C., Stocker, R.F., and Luo, L. (2001). Target neuron prespecification in the olfactory map of Drosophila. Nature *414*, 204–208.

Jefferis, G.S., Potter, C.J., Chan, A.M., Marin, E.C., Rohlfing, T., Maurer, C.R., Jr., and Luo, L. (2007). Comprehensive maps of Drosophila higher olfactory centers: spatially segregated fruit and pheromone representation. Cell *128*, 1187–1203.

Jinno, S., Klausberger, T., Marton, L.F., Dalezios, Y., Roberts, J.D., Fuentealba, P., Bushong, E.A., Henze, D., Buzsáki, G., and Somogyi, P. (2007). Neuronal diversity in GABAergic long-range projections from the hippocampus. J. Neurosci. *27*, 8790–8804.

Kuffler, S.W. (1953). Discharge patterns and functional organization of mammalian retina. J. Neurophysiol. *16*, 37–68.

Küppers, B., Sánchez-Soriano, N., Letzkus, J., Technau, G.M., and Prokop, A. (2003). In developing Drosophila neurones the production of gamma-amino butyric acid is tightly regulated downstream of glutamate decarboxylase translation and can be influenced by calcium. J. Neurochem. *84*, 939–951.

Kurtovic, A., Widmer, A., and Dickson, B.J. (2007). A single class of olfactory neurons mediates behavioural responses to a Drosophila sex pheromone. Nature *446*, 542–546.

Lai, S.L., Awasaki, T., Ito, K., and Lee, T. (2008). Clonal analysis of Drosophila antennal lobe neurons: diverse neuronal architectures in the lateral neuroblast lineage. Development *135*, 2883–2893.

Lee, T., and Luo, L. (1999). Mosaic analysis with a repressible cell marker for studies of gene function in neuronal morphogenesis. Neuron *22*, 451–461.

Liang, L., and Luo, L. (2010). The olfactory circuit of the fruit fly Drosophila melanogaster. Sci China Life Sci *53*, 472–484.

Manoli, D.S., Foss, M., Villella, A., Taylor, B.J., Hall, J.C., and Baker, B.S. (2005). Male-specific fruitless specifies the neural substrates of Drosophila courtship behaviour. Nature *436*, 395–400.

Marin, E.C., Jefferis, G.S.X.E., Komiyama, T., Zhu, H., and Luo, L. (2002). Representation of the glomerular olfactory map in the Drosophila brain. Cell *109*, 243–255.

Melzer, S., Michael, M., Caputi, A., Eliava, M., Fuchs, E.C., Whittington, M.A., and Monyer, H. (2012). Long-range-projecting GABAergic neurons modulate inhibition in hippocampus and entorhinal cortex. Science *335*, 1506–1510.

Miyamichi, K., Amat, F., Moussavi, F., Wang, C., Wickersham, I., Wall, N.R., Taniguchi, H., Tasic, B., Huang, Z.J., He, Z., et al. (2011). Cortical representations of olfactory input by trans-synaptic tracing. Nature *472*, 191–196.

Nagel, G., Brauner, M., Liewald, J.F., Adeishvili, N., Bamberg, E., and Gottschalk, A. (2005). Light activation of channelrhodopsin-2 in excitable cells of Caenorhabditis elegans triggers rapid behavioral responses. Curr. Biol. *15*, 2279–2284.

Okada, R., Awasaki, T., and Ito, K. (2009). Gamma-aminobutyric acid (GABA)-mediated neural connections in the Drosophila antennal lobe. J. Comp. Neurol. *514*, 74–91.

Olsen, S.R., and Wilson, R.I. (2008a). Cracking neural circuits in a tiny brain: new approaches for understanding the neural circuitry of Drosophila. Trends Neurosci. *31*, 512–520.

Olsen, S.R., and Wilson, R.I. (2008b). Lateral presynaptic inhibition mediates gain control in an olfactory circuit. Nature *452*, 956–960.

Olsen, S.R., Bhandawat, V., and Wilson, R.I. (2010). Divisive normalization in olfactory population codes. Neuron *66*, 287–299.

Parnas, M., Lin, A.C., Huetteroth, W., and Miesenböck, G. (2013). Odor discrimination in Drosophila: from neural population codes to behavior. Neuron, this issue, 932–944.

Potter, C.J., Tasic, B., Russler, E.V., Liang, L., and Luo, L. (2010). The Q system: a repressible binary system for transgene expression, lineage tracing, and mosaic analysis. Cell *141*, 536–548.

Root, C.M., Masuyama, K., Green, D.S., Enell, L.E., Nässel, D.R., Lee, C.H., and Wang, J.W. (2008). A presynaptic gain control mechanism fine-tunes olfactory behavior. Neuron *59*, 311–321.

Ruta, V., Datta, S.R., Vasconcelos, M.L., Freeland, J., Looger, L.L., and Axel, R. (2010). A dimorphic pheromone circuit in Drosophila from sensory input to descending output. Nature *468*, 686–690.

Semmelhack, J.L., and Wang, J.W. (2009). Select Drosophila glomeruli mediate innate olfactory attraction and aversion. Nature *459*, 218–223.

Shepherd, G.M., Chen, W.R., and Greer, C.A. (2004). Olfactory Bulb. In The synaptic organization of the brain, G.M. Shepherd, ed. (Oxford: Oxford University Press).

Sherrington, C.S. (1906). The Integrative Action of the Nervous System, Reprint (New Haven: Yale University Press).

Silbering, A.F., Rytz, R., Grosjean, Y., Abuin, L., Ramdya, P., Jefferis, G.S., and Benton, R. (2011). Complementary function and integrated wiring of the evolutionarily distinct Drosophila olfactory subsystems. J. Neurosci. *31*, 13357–13375.

Sosulski, D.L., Bloom, M.L., Cutforth, T., Axel, R., and Datta, S.R. (2011). Distinct representations of olfactory information in different cortical centres. Nature *472*, 213–216.

Stocker, R.F., Lienhard, M.C., Borst, A., and Fischbach, K.F. (1990). Neuronal architecture of the antennal lobe in Drosophila melanogaster. Cell Tissue Res. *262*, 9–34.

Stockinger, P., Kvitsiani, D., Rotkopf, S., Tirián, L., and Dickson, B.J. (2005). Neural circuitry that governs Drosophila male courtship behavior. Cell *121*, 795–807.

Su, C.Y., Menuz, K., and Carlson, J.R. (2009). Olfactory perception: receptors, cells, and circuits. Cell *139*, 45–59.

Su, C.Y., Martelli, C., Emonet, T., and Carlson, J.R. (2011). Temporal coding of odor mixtures in an olfactory receptor neuron. Proc. Natl. Acad. Sci. USA *108*, 5075–5080.

Tanaka, N.K., Awasaki, T., Shimada, T., and Ito, K. (2004). Integration of chemosensory pathways in the Drosophila second-order olfactory centers. Curr. Biol. *14*, 449–457.

Tian, L., Hires, S.A., Mao, T., Huber, D., Chiappe, M.E., Chalasani, S.H., Petreanu, L., Akerboom, J., McKinney, S.A., Schreiter, E.R., et al. (2009). Imaging neural activity in worms, flies and mice with improved GCaMP calcium indicators. Nat. Methods *6*, 875–881.

van der Goes van Naters, W., and Carlson, J.R. (2007). Receptors and neurons for fly odors in Drosophila. Curr. Biol. *17*, 606–612.

Vogel, A., and Venugopalan, V. (2003). Mechanisms of pulsed laser ablation of biological tissues. Chem. Rev. *103*, 577–644.

Vosshall, L.B., and Stocker, R.F. (2007). Molecular architecture of smell and taste in Drosophila. Annu. Rev. Neurosci. *30*, 505–533.

Wang, L., and Anderson, D.J. (2010). Identification of an aggression-promoting pheromone and its receptor neurons in Drosophila. Nature *463*, 227–231.

Wang, J.W., Wong, A.M., Flores, J., Vosshall, L.B., and Axel, R. (2003). Two-photon calcium imaging reveals an odor-evoked map of activity in the fly brain. Cell *112*, 271–282.

Wong, A.M., Wang, J.W., and Axel, R. (2002). Spatial representation of the glomerular map in the *Drosophila* protocerebrum. Cell *109*, 229–241.

Yu, J.Y., Kanai, M.I., Demir, E., Jefferis, G.S., and Dickson, B.J. (2010). Cellular organization of the neural circuit that drives Drosophila courtship behavior. Curr. Biol. *20*, 1602–1614.

Neuron, Volume *79*

Supplemental Information

GABAergic Projection Neurons Route Selective Olfactory Inputs to Specific Higher-Order Neurons

Liang Liang, Yulong Li, Christopher J. Potter, Ofer Yizhar, Karl Deisseroth, Richard W. Tsien, and Liqun Luo

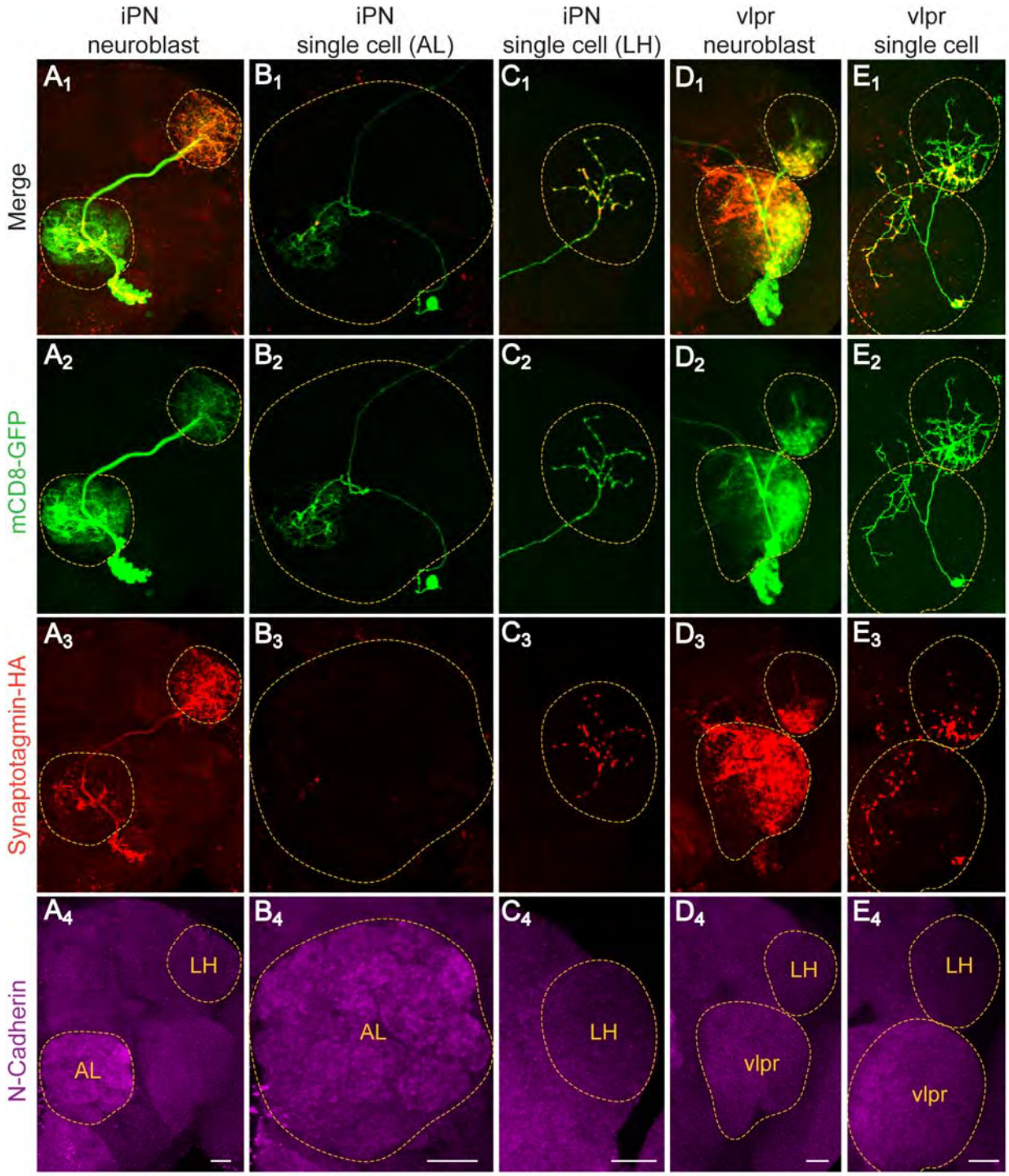

Figure S1. MARCM Analysis of Mz699+ iPNs and vlpr Neurons, Related to Figure 1
Representative MARCM clones for an iPN neuroblast (A_1-A_4), an iPN single cell arborization in the antennal lobe (B_1-B_4) and the lateral horn (C_1-C_4), a vlpr neuroblast (D_1-D_4) and a single vlpr neuron (E_1-E_4). *Mz699-GAL4* was used to drive *UAS-mCD8-GFP* and *UAS-Synaptotagmin-HA*. Green: anti-GFP staining; red: anti-HA staining; magenta: anti-N-Cadherin staining of the general neuropil. Row 1 shows the merge of the stained images in rows 2 and 3. Note that for

iPNs the synaptic vesicle marker Synaptotagmin-HA is weak and sparse in the antennal lobe, but strong in the lateral horn (A_3-C_3), indicating that the majority of the iPN output is in the lateral horn. The vlpr neurons have Synaptotagmin-HA labeling in both the lateral horn (LH) and vlpr neuropil (D_3-E_3) indicating these vlpr neurons may have output in both regions. However, the fine terminal arborizations that are free of Synaptotagmin-HA puncta are mostly present in the lateral horn but not in the vlpr neuropil, suggesting that the lateral horn is the major input to the vlpr neurons. The red channel in (B_1) and (B_3) are maximum projection from partial *z* stack to reveal the weak Synaptotagmin-HA staining. Scale, 20 μm.

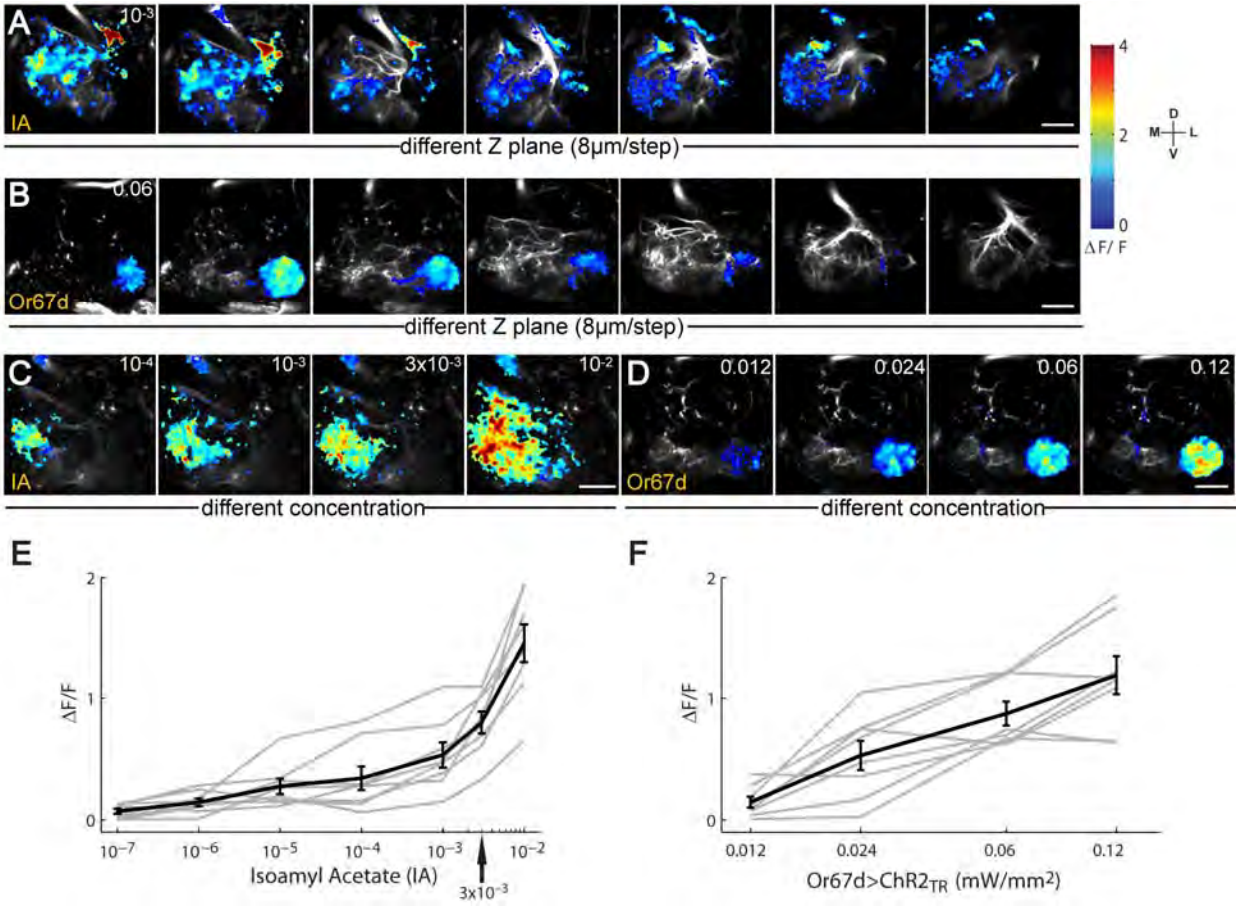

Figure S2. The iPN Responses to Olfactory Stimuli in the Antennal Lobe, Related to Figures 1 and 4

(A) The iPN response of a representative fly to 0.1% IA stimulation at a series of *z* planes every 8 μm across the antennal lobe. IA activates iPN responses in many parts of the antennal lobe. Due to the relatively sparse arborization of iPN dendrites, the glomeruli identities were not determined. Scale, 20 μm.

(B) The iPN response to optogenetically activating the Or67d ORNs (0.06 mW/mm^2) at a series of *z* planes every 8 μm across the antennal lobe. Ca^{2+} response is restricted to the large DA1 glomerulus.

(C) The peak ΔF/F of iPN dendrites of a representative fly in response to a series of IA concentrations (with 1 trial at each concentration, as 3 repeats caused strong adaptation at concentrations above 10^{-3}).
(D) The peak ΔF/F of iPN dendrites of a representative fly in response to optogenetically activating the Or67d ORNs at a series of light intensity.
(E) Peak ΔF/F of antennal lobe iPN responses to increasing concentration of IA (n=8, mean ± SEM). For each fly, the averaged ΔF/F at each concentration was calculated in the ROI defined by the response pattern at 10^{-2} IA of that fly. The odorant was delivered once at each concentration to avoid adaptation. The gray traces represent data from individual flies.
(F) Response of ΔF/F in the iPN dendrites to Or67d activation at different laser power (n=8, mean ± SEM). For each fly, the averaged ΔF/F at each concentration was calculated in the ROI defined by the response pattern at 0.12 mW/mm^2.
GCaMP imaging was performed in the *Or67d/Y;UAS-GCaMP3,QUAS-ChR2$_{TR}$; Mz699-Gal4/+* flies. 3 repeats were recorded consecutively for each data point unless otherwise stated, and the imaging sequence was from dorsal to ventral AL for the *z* stack, or from low to high stimulation strength for the concentration dependence.

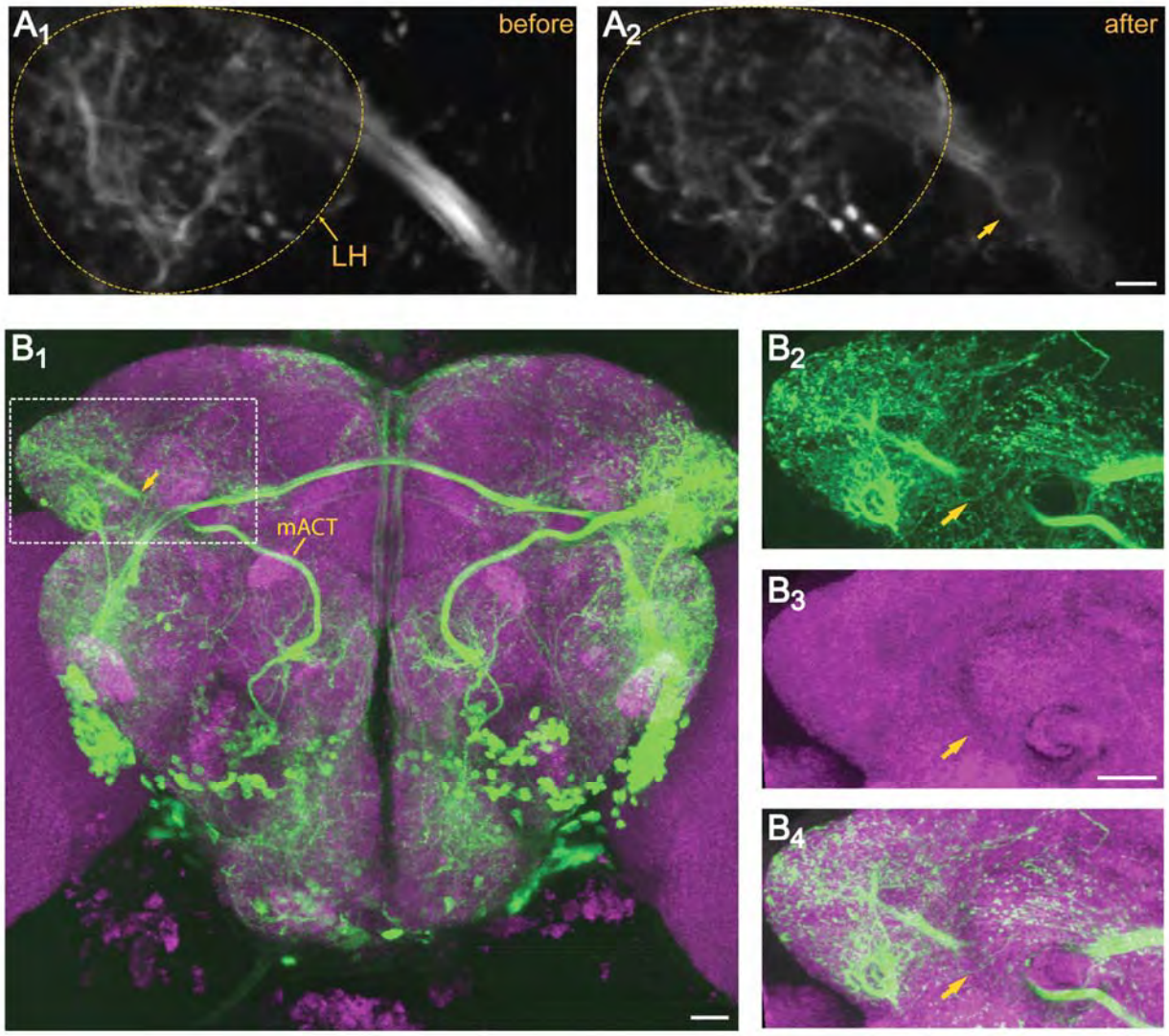

Figure S3. Validation of mACT Transection, Related to Figure 2
(A) Two-photon imaging of basal GCaMP signals immediately after mACT transection (A_2) compared with before (A_1). A cavitation bubble is clearly visible on the mACT (arrow). The lateral horn is outlined. Scale, 5 µm.
(B) *Post hoc* immunostaining confirmed that the mACT was successfully transected. (B_1) Confocal Z projection of the entire brain shows a disconnection in the mACT on the experimental hemisphere (left) compared with the intact mACT on the control hemisphere (right). (B_2-B_4) High magnification partial *z* projection of the region outlined in B_1. Green: anti-GFP staining; magenta: mAb nc82 staining. Arrows point to the site of laser transection. Scale, 20 µm.
Genotype for both panels: *Mz699-GAL4, UAS-GCaMP3*.

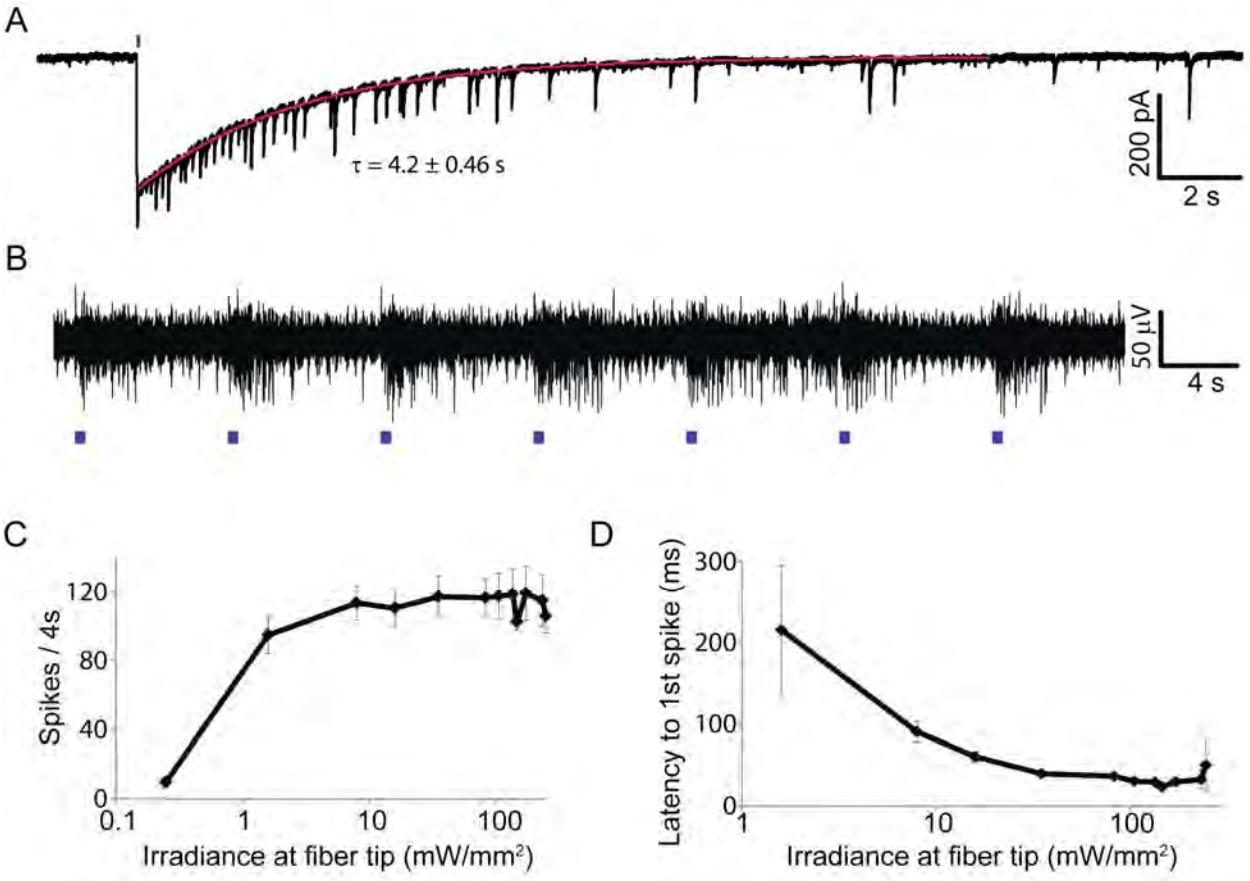

Figure S4. Photocurrent Properties and In Vivo Light Sensitivity of $ChR2_{TR}$, Related to Figure 4
(A) Voltage clamp recording from a cultured rat hippocampal neuron infected with pLenti CaMKIIα-$ChR2_{TR}$-EYFP virus. Red line denotes a monoexponential fit to the experimental

curve, from which the time constant of spontaneous decay (τ_{off}) can be calculated. The time constant displayed under the trace indicates the average τ_{off} (n = 5 cells). The blue bar indicates a 10-msec light pulse (470 nm±20, 5 mW/mm^2).
(B) In vivo extracellular recording from a mouse injected with the same virus as in (A). Recordings were performed using a tungsten electrode (FHC Inc.) located approximately 0.5mm below the tip of a 300 µm fiber. Blue bars indicate stimuli with 500 msec light pulses (473 nm, 3.54 mW/mm^2 at the fiber tip).
(C) Summary of multiple recordings in which 500 msec light pulses of varying irradiance were delivered as in (B). The number of spikes following each pulse was recorded and summarized across 3 recording sites. 1mW/mm^2 at the fiber tip corresponds with ~0.03 mW/mm^2 where the electrode was placed.
(D) Latency to first spike, calculated as the time from light onset. Longer latencies most likely resulted from accumulation of photocurrent during the light pulse.

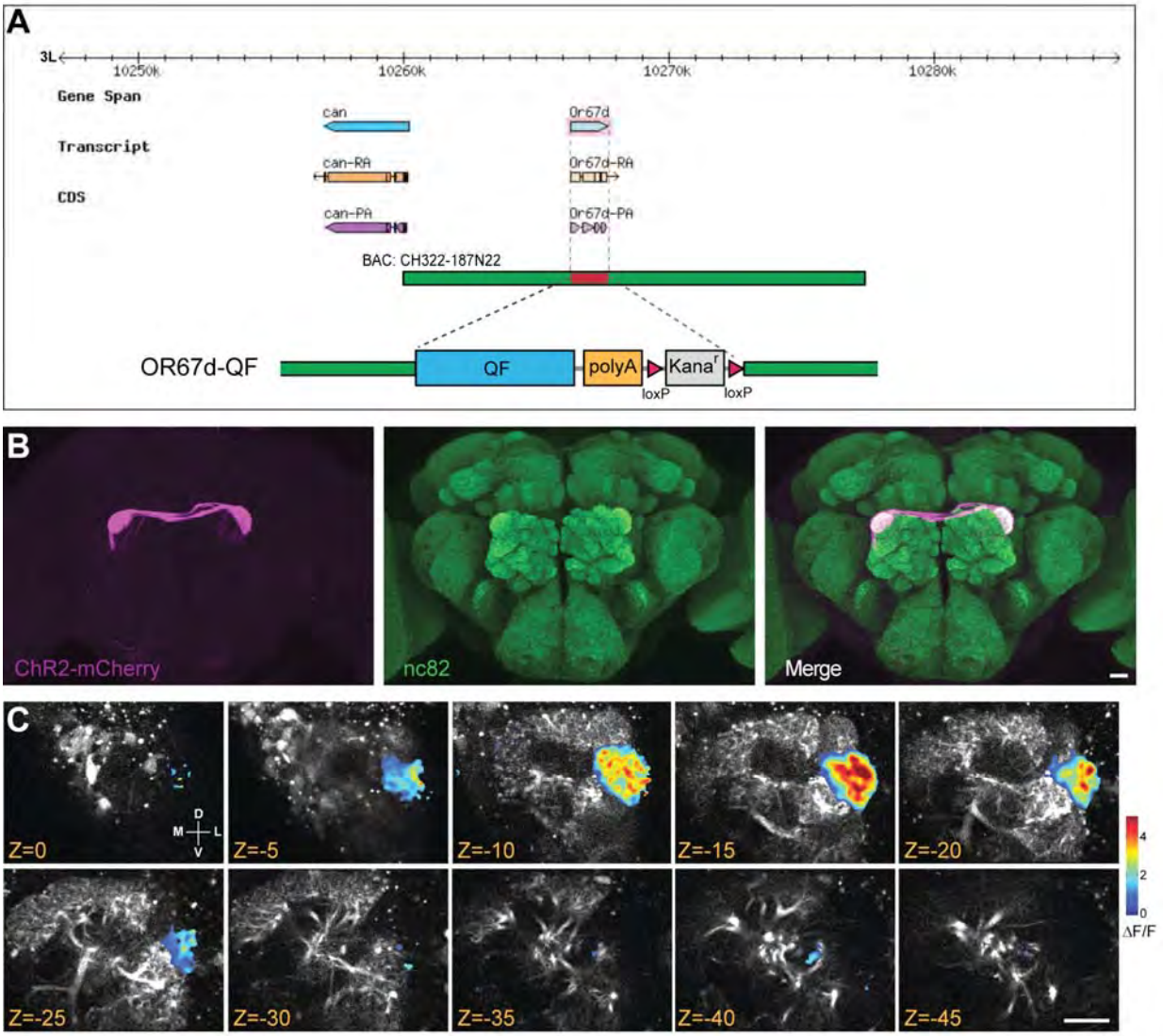

Figure S5. Characterization of *Or67d-QF* and *QUAS-ChR2$_{TR}$* Transgenes, Related to Figure 4

(A) Schematic of the *Or67d-QF* transgene. A region containing *QF-polyA-Kana^r* replaced the *Or67d* coding sequence in a 17.4 kb BAC clone (see Supplemental Experimental Procedures).

(B) ChR2$_{TR}$ from *QUAS-ChR2$_{TR}$* is specifically expressed in the DA1 glomerulus when driven by *Or67d-QF*. Magenta: anti-DsRed staining for mCherry fused to ChR2$_{TR}$; green: mAb nc82 staining. Scale, 20 µm.

(C) Optogenetic stimulation of Or67d ORNs specifically activates the DA1 PNs. ChR2$_{TR}$ is expressed in the Or67d ORNs using the Q system as in panel B. ~90 PNs innervating >40 glomeruli are labeled by the *GH146-GAL4, UAS-GCaMP3*. In the antennal lobe, light activation induces Ca^{2+} signal only in the DA1 PN dendrites. Ca^{2+} signals were imaged at a series of *z* planes every 5 µm. All the ΔF/F panels shown here were from the 2nd frame after blue laser stimulation. Scale, 20 µm. In this experiment only, a different sample preparation was used (modified after Wang et al., 2003), in which imaging was performed on a dissected brain with antennae attached.

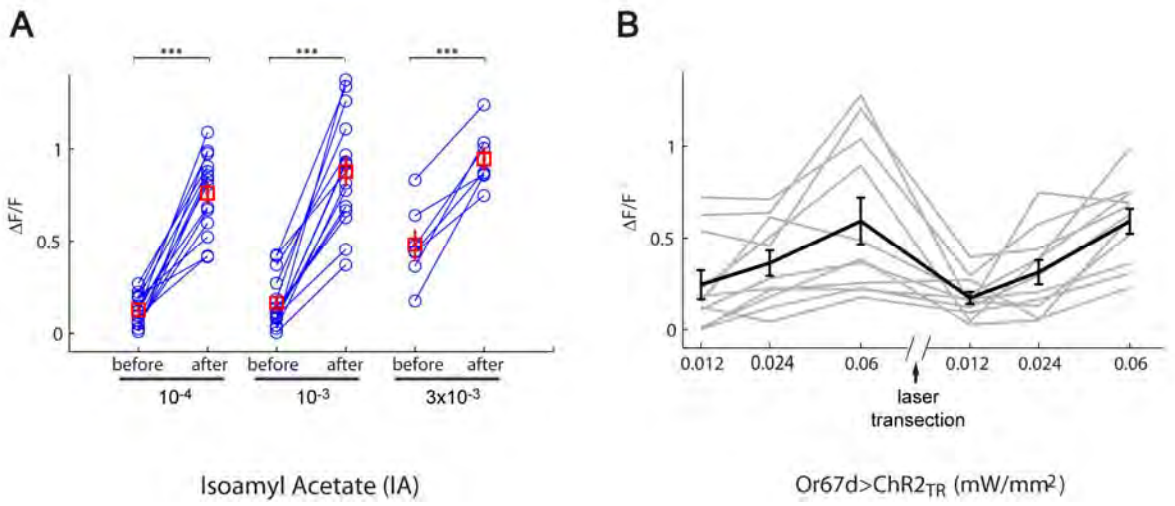

Figure S6. Testing the Concentration Dependence of the vlpr Response in the Lateral Horn, Related to Figures 2 and 4

(A) At three different IA concentrations, the vlpr response increased after mACT transection compared to before transection. The middle pair is a re-plot of Figure 2F$_1$ to aid comparison. At the highest IA concentration ($3x10^{-3}$), the vlpr response appears higher than that of 10^{-3} IA before mACT transection, suggesting that the iPNs suppression is incomplete in intact flies. At the lowest concentration (10^{-4}), 2/16 flies did not show significant vlpr response even after mACT ablation, and therefore were not included in the quantification (n=14, paired t-test). In all cases, after ablating the mACT, the vlpr neuron responses to IA stimuli were further increased.

(B) The lateral horn vlpr response to different levels of optogenetic stimulation of Or67d before and after mACT transection. No significant change of vlpr response was found before and after mACT transection for each stimulation condition (n=11). We also performed imaging experiment under 0.024 mW/mm^2 in dedicated flies (n=5), and no significant changes were caused by the mACT transection (data not shown). Error bars represent ±SEM.

SUPPLEMENTAL EXPERIMENTAL PROCEDURES

Genetics and Molecular Biology

Drosophila melanogaster were grown in standard media at 25°C. *Mz699-GAL4* (Ito et al., 1997), *UAS-GCaMP3* (Tian et al., 2009), *UAS-Dicer2* (Dietzl et al., 2007) were kindly provided by Drs. Tzumin Lee, Loren Looger, and Barry Dickson, respectively. *UAS-Gad1-RNAi* was obtained from the Vienna *Drosophila* RNAi Center (transformant ID #32344).

To construct *Or67d-QF* by BAC recombineering, a 17.4 kb BAC clone (#CH322-187N22) contained in the *attB-P[acman]-CmR-BW* vector (Venken et al., 2009) was obtained from the BACPAC Resources Center (Children's Hospital Oakland Research Institute). A sub region containing QF cDNA, SV40 polyA and loxP flanked $Kana^r$ gene was PCR amplified, and recombined into the BAC vector to replace the entire Or67d coding sequence (CDS), with the 50 bp immediately upstream and downstream of Or67d CDS as the homologous arms. The modified BAC construct was sequence verified and used to generate a transgenic fly line by random insertion (BestGene Inc). The transgene was mapped to the X chromosome and its expression pattern was verified by using the reporter line *QUAS-mCD8GFP* (Potter et al, 2010).

To generate $ChR2_{TR}$, we mutated the codon-optimized *ChR2(H134R)-EYFP* construct using a QuickChange IIXL mutagenesis kit to introduce the C128T mutation. Primer sequences were previously described (Berndt et al., 2009). The resulting construct was cloned into *pLenti-CaMKIIα* backbone for expression in excitatory pyramidal neurons. To construct *pQUAST-$ChR2_{TR}$-mCherry* (abbreviated as *QUAS-$ChR2_{TR}$* in the text), the *hChR2-mCherry* (Zhang et al., 2007) was PCR amplified and inserted into *pQUAST-attB* vector to generate the *pQUAST-attB-hChR2-mCherry*. The mutant *$ChR2_{TR}$* was PCR amplified and used to replace *hChR2* in *pQUAST-attB-hChR2-mCherry*. The resulting construct was used to generate transgenic flies through PhiC31-mediated integration at the *attP24* locus on Chromosome II (Groth et al., 2004).

MARCM Analysis and Immunostaining

The MARCM experiment was performed with flies of the following genotype: *UAS-mCD8GFP, UAS-Synaptotagmin-HA, hs-flp/+; FRT40A, tub-GAL80/FRT40A; Mz699-GAL4/+*. Parental flies were transferred to fresh vials every 24 hours. All the collected vials from day 1 to day 6 were heat-shocked on day 7 at 37°C for one hour. The heat-shock induced Flp expression resulted in mitotic recombination between the FRT chromosome arms in some of the dividing cells so that one daughter cell and its progeny lost *tub-GAL80* and became labeled. Brains were dissected from the appropriate genotypes 3~5 days after eclosion.

Brain dissection and immunostaining followed previously described procedures (Wu and Luo, 2006). Primary antibodies used were rat anti-N-Cadherin (1:40, DN-EX no. 8, Developmental Studies Hybridoma Bank (DSHB)), Mouse nc82 (DSHB, 1:25), Mouse anti-HA (1:100, 12CA5, gift from K. Wehner), Rabbit anti-Dsred (1:1000, Clontech), Rat anti-mCD8a (1:200, Invitrogen), Rabbit anti-GFP (1: 1000, Molecular Probes), Mouse anti-GFP (1:1000, sigma), Rabbit anti-GABA (1:200, Sigma). Secondary antibodies were used at 1:200, and included goat anti-rabbit FITC (Jackson ImmunoResearch Laboratories (JIRL)), goat anti-mouse Cy3 (JIRL), goat anti-rat Cy5 (JIRL), goat anti-rabbit Alexa Fluor 647 (Molecular Probes (MP)), goat anti-rat Alexa Fluor 488 (MP).

Confocal images of the immunostained brains were taken with a Zeiss 510 confocal microscope. Images shown in Figure 1B-E were the maximum projection of the whole stack of the fly brain. Images of GABA staining were from the representative single z section. The

GABA immunostaning positive cell numbers were counted throughout the z stack using the 'cell counter' plugin in ImageJ (NIH).

Preparing Flies for Ca^{2+} Imaging

Adult male flies of the appropriate genotype were transferred to a new vial 0~2 day after eclosion, and then kept at room temperature for 8~12 days. Each experimental animal was gently knocked down onto an ice-cold metal plate for ~20 sec until the fly no longer moved. The anesthetized fly was then transferred to the dissection/imaging chamber with forceps holding the wings as described (Olsen et al., 2010). Briefly, a tin foil with a hole of about 0.8 mm by 0.4 mm was taped onto a circular opening at the bottom of a chamber made from aluminum. The dorsal part of the fly head and thorax was inserted into the tin foil hole, while keeping its antennae exposed beneath the tin foil. The fly was further secured by applying the silicone adhesive (Kwik-Sil adhesive, World Precision Instruments) surrounding the eyes, neck, thorax and the tin foil. After fine adjustment of the fly position, the chamber was left in a humidified container for 10 min to allow the adhesive to cure. At this stage, flies were usually alert and displayed leg movement. We used sharp forceps to cut muscles 1 and 2 underneath the proboscis to reduce the brain movement. The two front legs were sometimes removed to expose the proboscis. Finally, we gently removed the cuticle covering the lateral horn or antennal lobe regions as well as the air sac and the fat bodies underneath the cuticle and cut muscle 16. The fly brain dissection was performed in ice-cold adult-like hemolymph (ALH) without Ca^{2+}. The regular ALH is composed of (in mM) 108 NaCl, 5 KCl, 5 Hepes, 5 Trehalose, 5 sucrose, 26 $NaHCO_3$, 1 NaH_2PO_4, 2 $CaCl_2$ and 1~2 $MgCl_2$, osmolarity adjusted to 275 mOsm, as previously described (Ruta et al, 2010). 5% CO_2 / 95% O_2 was continuously bubbled to maintain ALH at pH 7.3. Imaging was performed with ALH containing Ca^{2+} perfused at 0.5 ml/min.

For odor delivery, carbon filtered house air was first humidified by bubbling through a water-containing flask, followed by splitting into two branches with a flow rate at 500 ml/min each. Control odor [mineral oil (Sigma, 69794) or H_2O] or an experimental odor (60 µl) absorbed on a filter paper was placed inside a glass Pasteur pipette connected to the end of an air branch, and switched through solenoid valves. The ends of pipettes were connected to parallel inner diameter tubes (1/16 inch) positioned ~1cm from the fly antennae. Odorants used in the experiment are: apple cider vinegar (Heinz), isoamyl acetate (Sigma, W205532), and phenylacetic acid (Sigma, P16621). Odors were diluted in mineral oil or H_2O. The solenoid valves were controlled through Triggersync plugin (Prairie Technologies) and synchronized with the image acquisition system by data acquisition boards (National Instruments). All odorant tubes and solenoid valves were made from Teflon.

Data Analysis

With manual fly brain immobilization, each fly may be mounted with slightly different angles. In addition, no reliable landmarks at the lateral horn neuropil could be used to identify and register similar focal plane or neural processes across different brain hemispheres or flies. Therefore, our quantitative analysis mostly involves comparing calcium signals from the same imaging focal plane (*z*) in the same lateral horn before and after mACT transection. Image processing procedures described in detail below were performed mostly to reduce noise inherent to neuropil imaging from single *z* planes.

The GCaMP3 fluorescence images taken at the same *z* plane, including images from before and after mACT transection, were registered using Turboreg ImageJ plugin (Thevenaz et

al., 1998) facilitated by a batch registration plugin (Nimmerjahn et al., 2009). A Gaussian blur filter of $\sigma=2$ was then applied to each image frame. A mean background value from regions without GCaMP3 presence was subtracted to correct the fluorescence intensity F. For each pixel, we calculated the normalized fluorescence intensity change as $\Delta F/F=(F-F_0)/F_0$, where F_0 is the baseline fluorescence averaged from the 10 frames before odor delivery. ΔF is considered as significant and carried to further analysis if it is beyond 3x standard deviation calculated from the same 10 frames. We also applied a temporal filter to the image sequence: for each pixel, ΔF is kept as none zero only if the value from the same pixel is positive in at least one of its two adjacent frames.

To create the region of interest (ROI) from calcium signals after transection, the $\Delta F/F$ images from the first 3 imaging frames after Ca^{2+} response onset (which covered the response peak) were averaged to obtain $(\Delta F/F)_{avg}$. A further average across the three repeats followed by a 3×3 median filter gave rise to $(\Delta F/F)_{repeat\ avg}$. Only $(\Delta F/F)_{avg}$ with a positive value in at least two out of the three repeats were included for further analysis. We then converted the $(\Delta F/F)_{repeat\ avg}$ to a binary image as the ROI. An individual after-transection ROI was created in such a way for each lateral horn.

We applied the after-transection ROI to the time-lapse movies (both before and after transection) and obtained the peak frame responses (normalized by the size of the ROI) for each repeat. For any given odor stimulus, the time to peak was invariant from experiment to experiment. The integrated $\Delta F/F$ is a sum of frame-averaged $\Delta F/F$ from the odor onset to 11 sec thereafter when $\Delta F/F$ decays back to baseline. Student's t-test was performed between 3 repeats of the responses before and after transection (Figure $2E_1$, E_2). For the grouped comparison of the peak or integrated $\Delta F/F$ across all flies, paired Student's t-test was performed with the before- and after- transection $\Delta F/F$ from the same hemisphere as a pair. As ROI is defined by the post-transection response area, the averaged $\Delta F/F$ in the ROI is biased slightly for the post-transection response if random noises contribute to the calcium signal. In addition, we chose imaging planes that bias towards showing the after-transection vlpr responses, therefore the odor responses in other focal planes of the lateral horn were not captured by the images we show.

To generate peak frame $\Delta F/F$ images shown in the figures, the peak frame $\Delta F/F$ values from 3 repeats were averaged, followed by a median filter of size 3 by 3 pixels. Pixels where calcium responses only appeared in 1 out of 3 repeats were not included. The dynamics of GCaMP3 $\Delta F/F$ signal were calculated based on grouped F in the ROI. All image processing after the registration step was performed in Matlab (Mathworks) with custom scripts. Two-way ANOVA analyses were carried out in Prism (Graphpad Software).

To calculate the spatial correlation coefficient between the before- and after-transection responses from the same hemisphere, $(\Delta F/F)_{repeat\ avg}$ was Gaussian blurred and then converted from 2-D matrices into 1-D vectors. All the '0's common to both 1-D vectors were removed. Pearson's correlation coefficient was calculated between the two 1-D vectors. The correlation coefficients between the experimental and control hemispheres from the same fly were paired when performing paired Student's t-test across different flies.

SUPPLEMENTAL REFERENCES

Berndt, A., Yizhar, O., Gunaydin, L.A., Hegemann, P., and Deisseroth, K. (2009). Bi-stable neural state switches. Nat Neurosci *12*, 229-234.

Dietzl, G., Chen, D., Schnorrer, F., Su, K.C., Barinova, Y., Fellner, M., Gasser, B., Kinsey, K., Oppel, S., Scheiblauer, S., *et al.* (2007). A genome-wide transgenic RNAi library for conditional gene inactivation in Drosophila. Nature *448*, 151-156.

Groth, A.C., Fish, M., Nusse, R., and Calos, M.P. (2004). Construction of transgenic Drosophila by using the site-specific integrase from phage phiC31. Genetics *166*, 1775-1782.

Ito, K., Sass, H., Urban, J., Hofbauer, A., and Schneuwly, S. (1997). GAL4-responsive UAS-tau as a tool for studying the anatomy and development of the Drosophila central nervous system. Cell and tissue research *290*, 1-10.

Nimmerjahn, A., Mukamel, E.A., and Schnitzer, M.J. (2009). Motor behavior activates Bergmann glial networks. Neuron *62*, 400-412.

Olsen, S.R., Bhandawat, V., and Wilson, R.I. (2010). Divisive normalization in olfactory population codes. Neuron *66*, 287-299.

Thevenaz, P., Ruttimann, U.E., and Unser, M. (1998). A pyramid approach to subpixel registration based on intensity. IEEE transactions on image processing : a publication of the IEEE Signal Processing Society *7*, 27-41.

Tian, L., Hires, S.A., Mao, T., Huber, D., Chiappe, M.E., Chalasani, S.H., Petreanu, L., Akerboom, J., McKinney, S.A., Schreiter, E.R., *et al.* (2009). Imaging neural activity in worms, flies and mice with improved GCaMP calcium indicators. Nat Methods *6*, 875-881.

Venken, K.J., Carlson, J.W., Schulze, K.L., Pan, H., He, Y., Spokony, R., Wan, K.H., Koriabine, M., de Jong, P.J., White, K.P., *et al.* (2009). Versatile P[acman] BAC libraries for transgenesis studies in Drosophila melanogaster. Nat Methods *6*, 431-434.

Wang, J.W., Wong, A.M., Flores, J., Vosshall, L.B., and Axel, R. (2003). Two-photon calcium imaging reveals an odor-evoked map of activity in the fly brain. Cell *112*, 271-282.

Zhang, F., Wang, L.P., Brauner, M., Liewald, J.F., Kay, K., Watzke, N., Wood, P.G., Bamberg, E., Nagel, G., Gottschalk, A., *et al.* (2007). Multimodal fast optical interrogation of neural circuitry. Nature *446*, 633-639.